Carbohydrate Polymers 344 (2024) 122539

Contents lists available at ScienceDirect

Carbohydrate Polymers

journal homepage: www.elsevier.com/locate/carbpol

Valorization of citrus peel industrial wastes for facile extraction of extractives, pectin, and cellulose nanocrystals through ultrasonication: An in-depth investigation

Chandra Mohan Chandrasekar [a,*], Daniele Carullo [a], Francesca Saitta [a], Harini Krishnamachari [b], Tommaso Bellesia [a], Luca Nespoli [a], Enrico Caneva [c], Carlo Baschieri [c], Marco Signorelli [a], Alberto Giuseppe Barbiroli [a], Dimitrios Fessas [a], Stefano Farris [a], Diego Romano [a,*]

[a] Department of Food Environmental and Nutritional Sciences (DeFENS), University of Milan (UNIMI), Milan, Italy
[b] Centre for Food Technology, Anna University, Chennai, India
[c] UNITECH COSPECT: Comprehensive Substances characterisation via advanced sPECTtrometry, Milan, Italy

ARTICLE INFO

Keywords:
Citrus wastes
Ultrasonication
Pectin
Microcellulose
Nanocellulose
Structural analysis

ABSTRACT

In this work we developed an eco-friendly valorisation of Citrus wastes (CWs), through a solvent-assisted ultrasonication extraction technique, thus having access to a wide range of bio-active compounds and polysaccharides, extremely useful in different industrial sectors (food, cosmetics, nutraceutical). Water-based low-amplitude ultrasonication was examined as a potential method for pectin extraction as well as polar and non-polar citrus extractives (CEs), among which hesperidin and triglycerides of 18 carbon fatty acids were found to be the most representative ones. In addition, citric acid:glycerol (1:4)-based deep eutectic solvent (DES) in combination with ultrasonic extraction was utilized to extract microcellulose (CMC), from which stable cellulose nanocrystals (CNCs) with glycerol-assisted high amplitude ultrasonication were obtained. The physical and chemical properties of the extracted polysaccharides (pectin, micro and nanocellulose) were analysed through DLS, ζ-potential, XRD, HP-SEC, SEM, AFM, TGA-DSC, FTIR, NMR, and PMP-HPLC analyses. The putative structure of the extracted citrus pectin (CP) was analysed and elucidated through enzyme-assisted hydrolysis in correlation with ESI-MS and monosaccharide composition. The developed extraction methods are expected to influence the industrial process for the valorisation of CWs and implement the circular bio-economy.

1. Introduction

CWs represent a substantial by-product of the citrus fruit processing industry, comprising the outer rind, or peel, of fruits like oranges, lemons, and grapefruits (Humerez-Flores et al., 2022; M. Mariño et al., 2015; Pasarin et al., 2023). This residual material, often overlooked in the past, has garnered significant attention in recent years due to its potential for sustainable utilisation. Rich in bioactive compounds, essential oils, and diverse phytochemicals, CWs possess considerable value beyond its primary role as a flavourful outer layer (Singh et al., 2021). This waste stream not only presents opportunities for the extraction of essential oils used in various industries, but also harbours the potential for producing biofuels, pectin, and cellulose fibres (Humerez-Flores et al., 2022; M. Mariño et al., 2015). Moreover, its high content of antioxidants and antimicrobial agents has led to exploration in fields as diverse as food preservation, nutraceuticals, and even pharmaceuticals (Singh et al., 2021).

As the global push towards circular economy practices gains momentum, understanding the multifaceted potential of CWs is a pivotal step towards more sustainable and resource-efficient industrial processes. A range of valorisation methods have been developed, aiming to extract, transform, and repurpose these components into high-value products. These methods encompass a diverse array of techniques, including extraction processes for essential oils and bioactive

Abbreviations: CP, Citrus Pectin; CEs, Citrus extractives; CMC, Citrus Microcellulose; CNCs, Cellulose Nanocrystals; PCA, Principal Component Analysis; DES, Deep Eutectic Solvent; XRD, X-ray Diffraction; HPLC, High Performance Liquid Chromatography; HP-SEC, High Performance Size Exclusion Chromatography; FTIR, Fourier Transform Infrared Spectroscopy; AFM, Atomic Force Microscopy; SEM, Scanning Electron Microscopy; TGA, Thermogravimetric Analysis; DSC, Differential Scanning Calorimetry; NMR, Nuclear Magnetic Resonance; ESI-MS, Electrospray Ionisation Mass Spectroscopy.

* Corresponding authors.

https://doi.org/10.1016/j.carbpol.2024.122539
Received 3 May 2024; Received in revised form 19 July 2024; Accepted 22 July 2024
Available online 23 July 2024

compounds, enzymatic and microbial transformations to produce value-added chemicals, as well as biotechnological approaches for the synthesis of biofuels and other renewable materials. The exploration of these valorisation strategies not only addresses the pressing need for sustainable waste management, but also unlocks a myriad of economic and environmental benefits, positioning CWs as a promising resource for developing a circular economy (Du et al., 2024; Mathias et al., 2019; Panwar et al., 2023; Rajulapati et al., 2021; Singhal & Swami Hulle, 2022).

Deep eutectic solvents (DES) represent a captivating class of solvents that have garnered significant attention in recent years for their exceptional versatility and sustainability. Unlike conventional solvents, DES are composed of a eutectic mixture of two or more components, typically a hydrogen bond donor and acceptor, which form a eutectic point at a lower melting temperature than each component. This unique property imparts DES with a remarkable ability to dissolve a wide range of compounds, including polar and non-polar substances. DES has found applications across various fields, including chemistry, biotechnology, and materials science, owing to their low toxicity, biodegradability, and environmentally benign nature. Their tuneable properties and ability to replace conventional volatile organic solvents make DES a promising alternative for greener and more sustainable processes (Kang et al., 2023; Mao et al., 2023; Rico et al., 2022; Varilla-Mazaba et al., 2022).

Ultrasonication-assisted extraction has emerged as a cutting-edge technique in the realm of pectin extraction, offering a highly efficient and environmentally friendly method for obtaining this vital polysaccharide from plant materials (Panwar et al., 2023). Pectin, a complex carbohydrate found in the cell walls of various fruits and vegetables, possesses a wide range of functional properties that make it invaluable in industries such as food, pharmaceuticals, and cosmetics. By subjecting plant matrices to ultrasonication (i.e., high-frequency sound waves) facilitates the release of pectin from cell walls, resulting in a more rapid and effective extraction process compared to conventional methods. Ultrasonication also stands at the forefront of cellulose and nanocellulose extraction, enabling also the breakdown of cellulose at the nanoscale (Al Jitan et al., 2022; M. Mariño et al., 2015). This method offers precise control over particle size and morphology, resulting in nanocellulose fibres with tailored characteristics for myriad of applications, spanning from advanced materials and biomedical engineering to sustainable packaging and environmental remediation. From the above-mentioned observations: 1) we hypothesised that the solvent-based ultrasonication method could effectively extract both polysaccharides and extractives from the citrus industrial wastes, 2) we also hypothesised that enzyme-based hydrolysis of branched polysaccharides followed by mass spectrometric fragmentation analysis would provide in-depth insight into the elucidation of its probable structure.

The main aim of the present work is to obtain extractives, pectin, cellulose, and nanocellulose from citrus industrial wastes through the solvent-assisted ultrasonic extraction process to develop an eco-friendly valorisation method. The extracted extractives, pectin, cellulose, and nanocellulose were physically and chemically characterised. Moreover, the putative structure of the extracted CP was also elucidated through enzyme-assisted hydrolysis and electrospray ionisation mass spectroscopic analysis.

2. Materials and methods

2.1. Raw materials

CWs were provided by the citrus fruit processing industry Ortogel SPA (Belpasso, Catania, Italy). All the monosaccharide standards and chemicals (purity: > 95 %), as well as the Endo-PG (Endo polygalacturonase) EC 3.2.1.15 from *Aspergillus niger*, were purchased from Merck, (Darmstadt, Germany). The rhamnogalacturonan endolyase [EC 4.2.2.23], and *exo*-polygalacturonase [Exo-PG, EC 3.2.1.67] enzymes were purchased from Creative Enzymes (Shirley, NY, USA).

2.2. Pretreatment of CWs

The detailed valorisation procedures are depicted in the flowchart (Fig. S1). One kilogram of CWs was washed thrice with 1 L of water and then filtered. The liquid filtrate was dried to recover any excess citric acid residues. The filtered solid CW was dried in an air oven at 60 °C to constant weight. The dried CW was ground to fine powder of average particle size ~278 ± 60 μm. The ground CW powder was analysed for its chemical constituents as per the methods described in our previous work with some modifications (Harini & Chandra Mohan, 2020). The lignin content of the samples was determined using the TAPPI standard method T 222 om-88 (Tappi, 1988) by reaction with 72 % (*w*/w) sulfuric acid. The polar and non-polar extractives of CW were extracted using the soxhlet extraction method with 450 mL of ethanol and n-hexane (3 h extraction in each solvent separately), respectively. The cellulose content was estimated through the method described by (Updegraff, 1969), and the pectin content of the sample was analysed using Cu2+ ion precipitation, followed by UV-VIS spectrophotometric analysis as described by (F. Wang et al., 2021).

2.3. Ultrasonic extraction of CP and CEs

The fine powder of CW was subjected to ultrasonic solvent extraction with deionised water in a UP400S (power max = 400 W; frequency = 24 kHz) ultrasonic device (Hielscher, Teltow, Germany) equipped with a cylindrical titanium sonotrode (mod. H14, tip Ø 14 mm, amplitude max = 125 μm; surface intensity = 105 W cm^{-2}). A central composite design (CCD) of experiments was constructed with different solid-to-solvent ratios, ultrasonic amplitudes, and ultrasonication time as independent variables (input), whereas yield of pectin and polar and non-polar extractives were selected as dependent variables (output). The CCD summary and the set of experiments were given in supplementary data (Tables S1 and S2, respectively). After the ultrasonication time, the resultant solution was centrifuged (Eppendorf Centrifuge Model: 5804 R, Germany) at 2000 rpm (514.28 × 10^{-5} g) for 10 min to remove insoluble residues (rich in cellulose and extractives). The supernatant was subjected to precipitation with ice-cold ethanol to extract the water-dissolved pectin. The precipitated pectin was isolated by centrifugation at 3000 rpm (1157.13 × 10^{-5} g) for 10 min. The isolated pectin pellet was washed three times with ethanol to remove any associated polar extractives; the resultant pectin was freeze-dried, weighed, and stored at 4 °C for further characterisation. After pectin extraction, the insoluble residue (rich in cellulose, polar, and non-polar extractives) was subjected to consecutive solvent extractions with ethanol (to remove polar extractives) and hexane (to remove non-polar extractives) at 40 °C for 24 h. After the extraction process, the final residue (rich in cellulose) was filtered and stored at 4 °C for further processing. Then, the extracted extractives were condensed with a rotary evaporator (KNF RC600, Freiburg, Germany) and weighed. The percentage yield of pectin and extractives was calculated gravimetrically by comparing their weights with the weight of CWs.

2.4. Ultrasonic extraction of CMC and CNCs

For the extraction of CMC, the cellulose-rich fraction from the previous step was subjected to DES-assisted ultrasonic treatment to remove lignin. A 4:1 (glycerol:citric acid) solution with an average viscosity of 1459.4 mPa at 25 °C was used as a DES. A CCD of experiments was constructed with different DES soaking periods, ultrasonic amplitudes, and ultrasonication time as input factors, whereas the percentage of lignin removed from the cellulose-rich fraction was taken as output. The CCD summary and corresponding experiments are denoted in Tables S1 and S3, respectively. The sonicated solution was washed with 60 % ethanol to remove lignin through centrifugation at 3000 rpm (1157.13 × 10^{-5} g) for 15 min. The resultant pellet was washed thrice with 60 % ethanol and centrifuged to obtain pure CMC. The extracted CMC was

freeze-dried and stored at 4 °C for further analysis. The percentage of lignin removed was estimated by comparing the total lignin content of cellulose-rich fraction and extracted CMC.

For the extraction of CNCs, the extracted CMC was further processed through glycerol-assisted ultrasonication treatment. CMC was soaked in 70 % glycerol solution at 25 °C for different time periods under a magnetic stirrer operating at 600 rpm. A CCD of experiments was constructed with different glycerol soaking periods, ultrasonic amplitudes, and ultrasonic time as input factors and the average particle size in the solution was taken as a response. The CCD summary and corresponding experiments are denoted in Tables S1 and S4, respectively.

2.5. Characterization

2.5.1. Characteriation of polar and non-polar CEs

The chemical constituents present in polar and non-polar extractives of CW and their abundance were analysed through HPLC (Agilent 1290 Infinity II LC, Cernusco sul Naviglio, Italy), coupled with a triple quad mass spectrometer (ZenoTOF 7600 System (SCIEX) equipped with Turbo *V*™ Ion Source with ESI Probe). The chemical constituents' qualitative analysis was conducted by comparing their corresponding precursor mass spectral peaks with mass spectral databases (LipidBlast and LibraryView ver 1.4, database Natural Products HR-MS/MS Library). The quantity of the chemical constituents was estimated by calculating the area under the chromatographic peaks.

2.5.2. Characterisation of CP, CMC, and CNCs

2.5.2.1. Particle size and ζ-potential. Both size and ζ-potential of the samples were measured by photon correlation spectroscopy experiments using dynamic light scattering (DLS) and electrophoretic light scattering (ELS) analyses, respectively, using a LitesizerTM 500 (Anton Paar, Rivoli, Italy) system at neutral pH (Chandrasekar et al., 2024). The tests were carried out at 25 °C, with a stabilisation time of 60 s, and using viscosity (0.8872 cP) and refractive index (1.33) of water as reference values. The software Kalliope (Anton Paar, Rivoli, Italy) used the non-negative least squares algorithm to retrieve the size distribution.

2.5.2.2. Scanning Electron Microscopy (SEM). To acquire information on the surface morphology of the extracted polysaccharides, samples were placed on metallic stubs covered with carbon tape and sputter-coated with a thin layer of platinum (≈ 5 nm) using an Agar High-Resolution Sputter Coater (model 208RH). Micrographs were then retrieved using a SNE-Alpha instrument (SECENG, Korea) scanning electron microscope working at an accelerating voltage of 5 kV. SEM images were collected at different magnifications at an accelerating potential of 20 kV (Harini & Chandra Mohan, 2020).

2.5.2.3. Atomic Force Microscopy (AFM). In-depth morphological and size features of CNCs were determined using a ToscaTM 400 AFM (Anton Paar Italia Srl, Rivoli, Italy) in contact resonance amplitude imaging (CRAI) mode. Towards this goal, an Arrow-FMR-10 Force Modulation probe (Nanoworld, Neuchâtel, Switzerland) featuring a rectangular cantilever with a triangular free end and a tetrahedral tip with a typical height of 10–15 μm was used. Additionally, the tip radius of curvature is ~10 nm. The cantilever has a spring constant and resonance frequency of 2.8 N m^{-1} and 75 kHz, respectively. For the analyses, approximately 100 μL of diluted CNC water dispersion (~ 0.1 mg/mL) was dropped onto a mica disc substrate (Ted Pella Inc., Redding, California). Dimensional calculations and image editing were conducted via Digital surf Mountains Analysis Software (Rovera et al., 2023). The mean values reported for each CNCs dimension were calculated over at least five images, from which at least five measurements were taken.

2.5.2.4. Wide Angle X-ray Diffraction (WAXD). Information on samples crystallinity was obtained using a D8 Advance X-ray powder diffractometer (Bruker, USA) equipped with a one-dimensional Debye–Scherr camera, Cu Ka radiation (wavelength 0.1542 nm) operating at 40 kV and 35 mA. The crystallinity index (CI) was calculated using Eq. (1) by measuring the peak height of the crystalline region (I_{cry}) and the amorphous region (I_{am}) (Chandra Mohan et al., 2018; Harini & Chandra Mohan, 2020).

$$CI(\%) = \frac{I_{cry}}{I_{total}} \times 100 \quad (1)$$

where, I_{total} – Total area under XRD peaks [$I_{total} = I_{cry} + I_{am}$].

2.5.2.5. Thermogravimetric Analysis and Differential Scanning Calorimetry (TGA-DSC). The thermal degradation properties of the extracted polysaccharides were analysed by thermogravimetric analysis (TGA) coupled with differential scanning calorimetry (DSC). A Setaram TG-DSC111 (Lyon, France) was used to simultaneously record the TG trace (mass versus temperature) and the thermal effects (heat flow versus temperature). A typical sample mass of about 15 mg was placed into an aluminium crucible and heated from 25 °C to 500 °C at a scanning rate of 2 °C/min under nitrogen atmosphere. An empty aluminium crucible was used as a reference. Each run was repeated twice. All the TG traces reported in the figures were normalized to 100 mg of mass sample. Accordingly, the temperature derivative of the TG traces (DTG = dm (T)/dT) were expressed as mg•K^{-1}. Instead, all the DSC thermograms in the figures were normalized per mass of initial sample, hence expressing the heat flow as W•g^{-1}.

2.5.2.6. Solid-state Fourier Transform Infrared Spectroscopy (FTIR). FTIR analysis was performed using a Spectrum 100 instrument (Perkin Elmer Inc., Waltham, MA) coupled with an Attenuated Total Reflectance (ATR) accessory and a Ge/Ge crystal, fixed at an incident angle of 45°. All spectra were collected at a resolution of 4 cm^{-1} over a wavenumber range between 4000 cm^{-1} and 800 cm^{-1}, resulting from an average of 180 scans. A background scan of clean Ge crystal in the air was acquired before each scan (Rovera et al., 2023).

2.5.2.7. Solid-state ^{13}C Cross-Polarization Magic Angle Spinning (CP-MAS). CP-MAS spectra were collected at 125.76 MHz on an Avance 500 MHz NMR Spectrometer (Bruker Italia s.r.l., Milan, Italy), operating at a magnetic field of 11.7 T and equipped with a 4 mm MAS probe, spinning the sample at the magic angle up to 15 kHz, which, with the addition of high power 1H decoupling capability, allows the decrease or the elimination of homo and heteronuclear anisotropies. All the samples were prepared by packing them in Zirconia (ZrO2) rotors, closed with Kel-F caps (50 μL internal volume), and the MAS rate was optimised to 10 kHz after running some experiments in the 2–15 kHz range . Cross polarization spectra, under Hartmann–Hahn conditions, were recorded with a variable spin-lock sequence (ramp CPMAS) and a contact time of 1 ms, optimised into a range between 1 and 5 ms (Rovera et al., 2023).

2.5.2.8. Size Exclusion Chromatography (SEC). Molecular weight of samples was determined through a 515 Waters HPLC system coupled with Shodex OHpak LB-806 M column (for pectin) and PLgel MIXED-A column (for cellulose). The differential refractive index data was collected through the Wyatt Optilab T-rEX detector, and the multi-angle light scattering data was collected through the Wyatt Down Heleos detector. For pectin sampling, the mobile phase was 50 mM $NaNO_3$ with a 0.5 mL/min flow rate. The samples were lyophilised and dissolved at a 1.5 mg/mL concentration in the mobile phase. For cellulose sampling, the mobile phase was 0.9 % LiCl in DMAc with a 0.5 mL/min flow rate. The lyophilised samples were dissolved in the eluent (0.9 % LiCl in DMAc) using a solvent exchange procedure. Complete dissolution was achieved by stirring the solutions in a 2 mL Eppendorf overnight and at room temperature using a magnetic bar. The sample solutions were

filtered (Millipore Millex-GV PVDF 0.22 μm) before injection. The injection volume was 100 μL (Neckebroeck et al., 2021; Pitkänen & Sixta, 2020).

2.5.2.9. High Performance Liquid Chromatography (HPLC). The monosaccharide composition of extracted carbohydrates was analysed through PMP-labelled HPLC. The polysaccharide samples (10 mg) were dissolved in 1 mL of 3 M trifluoroacetic acid in a 5 mL ampoule and incubated at 130 °C for 2 h. The cooled reaction mixture was centrifuged at 2000 rpm (514.28×10^{-5} g) for 5 min and evaporated to dryness under reduced pressure to remove TFA. The hydrolysed and dried samples were redissolved in 1 mL of distilled water. The hydrolysed sample was labelled by adding 30 μL of NaOH (0.3 M) and 20 μL of PMP solution (0.5 M in methanol). The mixtures were incubated at 70 °C for 60 min, cooled to room temperature, and neutralised with 30 μL of HCl (0.3 M), 1 mL of trichloromethane was added, and, after *v*igorous shaking and layering, the organic phase was carefully removed and discarded. Before HPLC analysis, the aqueous layer was passed through a 0.45 μm syringe filter. Standard solutions of the Rha, Ara, Xyl, Man, Glc, Gal, Fuc, Rib, GlcA, GalA, di-GalA, and tri-GalA (0.1 μM) were also treated as described above. The PMP-labelled monosaccharides were analysed using an Agilent 1260 HPLC system (Waldbronn, Germany) consisting of a G1311C Quaternary pump, G1329B autosampler (0.1–100 μL), G1316A column oven (273–333 K), G1315D-DAD detector (190–950 nm), and 1260 Infinity II Analytical-Scale Fraction Collector. The analytical column was a TC-C18 column (4.6 mm × 250 mm, 5 μm; Agilent). The injection volume was 20 μL with an eluant flow rate of 1.0 mL/min at 35 °*C. mobile* phase A was 100 % acetonitrile, and mobile phase B was a mixture of distilled water and acetonitrile (90: 10, *v*/v) with 0.045 % KH_2PO_4–0.05 % triethylamine buffer (pH 7.5); gradient elution was performed at 94–94–88-88 % B with linear decreases at 0–4–5-20 min. The UV detection wavelength was set at 245 nm (Ai et al., 2016; Vojvodić Cebin et al., 2022).

2.5.2.10. Structural analysis of CP. Information on the chemical structure of pectin was carried out through enzyme-assisted degradation (Lemaire et al., 2020; McDonough et al., 2004; Yapo et al., 2007) with HPLC separation followed by electro spray ionisation – mass spectrometry (ESI-MS) (Lin et al., 2022; Xia et al., 2020). Ten mL of the extracted CP (100 mg/mL in 50 mM phosphate buffer [pH 5]) was mixed with 600 units of *endo*-polygalacturonase (Endo-PG, EC 3.2.1.15 from *Aspergillus niger*). The reaction mixture was incubated at 50 °C. Every 6 h, 0.5 mL of the reaction mixture was removed and heated to 105 °C for 10 min to arrest the reaction. Then, the solution was centrifuged at 5000 rpm (3214.25×10^{-5} g) for 5 min. This hydrolysed supernatant solution was subjected to the above-mentioned PMP labelled HPLC procedure supported with a 1260 Infinity II Analytical-Scale Fraction Collector. The different fractions of the eluted reaction mixture were collected and subjected to acid hydrolysis to find their monomeric constituents through PMP labelling. The structure of rhamnogalacturonan fractions of CP was analysed by double enzymatic hydrolysis followed by HPLC elution and ESI-MS. More specifically, 2 mL of the rhamnogalacturonan fractions (10 mg/mL in 50 mM phosphate buffer [pH 5]) was subjected to hydrolysis by 20 units of rhamnogalacturonan endolyase (Creative Enzymes [EC 4.2.2.23]) at 50 °C for 12 h. The hydrolysed solution was heated up to 105 °C for 5 min to arrest the reaction, and it was centrifuged at 5000 rpm (3214.25×10^{-5} g) for 5 min. The supernatant containing the hydrolysed fractions was again subjected to hydrolysis with 20 units of *exo*-polygalacturonase (Creative Enzymes [Exo-PG, EC 3.2.1.67]) at 40 °C for 12 h. The reaction was arrested by heating up to 105 °C for 5 min, and then the hydrolysed fraction was centrifuged at 5000 rpm (3214.25×10^{-5} g) for 5 min. The supernatant containing double hydrolysed fraction was eluted through HPLC coupled with a C-18 column and its separated fractions were analysed through ESI-MS as per the method followed by (Pasarin et al., 2023). The MS system was equipped with (Agilent Technologies, model 6224 TOF MS) detector. The system was calibrated using a mass reference solution (ESI-L Low concentration tunning mix, code G1969–85000, Agilent Technologies). MS detection was performed using an orthogonal TOF-MS coupled to an ESI source, with double spray needles for continuous infusion of the reference mass solution. The drying gas, heated to 350 °C, with a flow rate of 9.0 L/min nitrogen at a pressure of 40 psig (gauge pressure), was used to dissolve the solution drops. The spray was induced with a capillary voltage of 3500 *V*, and the fragmentation voltage was 100 V. The analyte solution (5 μL), filtered through 0.22 μm PTFE syringe filters, was injected directly into the MS. Data acquisition and qualitative processing were performed using Mass Hunter software, version B.04.00. The data acquisition range was set to 600–2000 *m/z*, with 9894 scans and a scan rate of 1 scan/s.

2.6. Statistical analyses

The analyses were conducted in five repetitions, and the average value for each analysis was evaluated from the repetitions. The results are represented in the form of mean ± standard error. Face Centered Central Composite Design (FC-CCD) experiments were developed for the extraction of CP, CEs, CMC, and CNCs (Table S1–4). These CCD data were analysed through the principal component analysis (PCA) framework using the Analyse-It software package to evaluate the influence and correlation of different treatments on the output parameters.

3. Results and discussion

3.1. Ultrasonic extraction of CP, CEs, CMC, and CNCs

The CCD for the extraction of CEs and CP is given in Table S2. The maximum yield of pectin (30.28 ± 1.92 % (*w*/w)) was achieved at 0.05 g/mL solid-to-solvent ratio, with an ultrasonication amplitude of 40 % and operating time of 10 min. The yield of pectin is higher than 19, 22, 7.4, and 29 % reported in orange peel [PEF extraction (Du et al., 2024)], grapefruit [DES extraction (X. Lin et al., 2024)], pumpkin biomass [microwave extraction (Košťálová et al., 2016)], and lemon peel [ultrasonic extraction (Panwar et al., 2023)], respectively. The ultrasonic extraction method gave a higher yield compared to the other extraction methods plausibly due to more effective disruption of plant cell wall owing to the cavitation phenomenon lying behind the ultrasound process. The corresponding yields of polar and non-polar extractives were estimated to be 6.91 ± 1.28 (w/w) and 2.98 ± 0.89 % (w/w), respectively. All the extraction data was analysed through PCA to acquire a better understanding of the extraction pattern and the influence of each input factor on the output. The mono-plot of the PCA gives a clear representation of the impact of each factor on the output. The length of each vector represents the amount of data that depends on the particular factor, and the angle between the input and output factors represents the dependency of the output on the input factors. The PCA correlation plot (Fig. S2 A), mono-plot (Fig. S2B), and bi-plot (Fig. S2C) of the pectin extraction data revealed that pectin yield is closely related to the ultrasonication time, with a positive correlation of 0.860 and moderately related to the ultrasonication amplitude, with a positive correlation of 0.274. The data analysis also revealed that an increase in the solid-to-solvent ratio negatively correlates (−0.353) to the pectin yield. These results imply that the extraction of pectin is positively affected by the ultrasonication amplitude and time. More importantly, an increase in treatment time plays a significant role in the extraction of pectin rather than the ultrasonication amplitude. These results also imply that an increase in solvent quantity plays a substantial role in the effective extraction of pectin through ultrasonication. The bi-plot represents the 2-D data of the 4-dimensional extraction data. Principal component 1 represents 52 % of the data, and the inclusion of principal component 2 represents 76.5 % of the data. The pectin yield for the desired run can be plotted within the data limitations of the principal

component bi-plot.

The PCA correlation plot (Fig. S3 A), mono-plot (Fig. S3B), and bi-plot (Fig. S3C) of the polar CEs extraction data revealed that polar CEs yield is equally related to both ultrasonication time (positive correlation of 0.460) and ultrasonication amplitude (positive correlation of 0.600). This analysis indicates that an increase in both ultrasonication time and amplitude impacts significantly ($P < 0.05$) the extraction of polar CEs. This phenomenon may be due to the high amount of polar CEs, which may be released to the solvent phase with nominal amplitude and time. The PCA correlation plot (Fig. S4 A), mono-plot (Fig. S4B), and bi-plot (Fig. S4C) of the non-polar CEs extraction data revealed that non-polar CEs yield is highly influenced by ultrasonication amplitude, with a positive correlation of 0.591 and moderately influenced by the ultrasonication time, with a positive correlation of 0.173. This significant impact of ultrasonication amplitude may be due to the power requirement for the disruption of the integrated cellular structure of CWs to release triglycerides and fatty acids. Both polar and non-polar CEs yields have a strong negative correlation with the to-solvent ratio; this may be ascribed to the need for a high solvent quantity for the dissolution of CEs.

The residual solid rich in cellulose was estimated to be 57.83 ± 2.36 % (*w*/w), and the remaining 2 % (w/w) will go as loss during purification wash. This cellulose-rich faction also contains 8.15 ± 1.24 % (w/w) lignin. This lignin fraction was removed by DES-assisted ultrasonication treatment. The CCD related to the lignin removal is tabulated in Table S3. The maximum removal of lignin (97.79 ± 3.59 %) was achieved in DES soaking time of 12 h, ultrasonication amplitude of 60 %, operating for the ultrasonication time of 15 min. The PCA correlation plot (Fig. S5 A), mono-plot (Fig. S5B), and bi-plot (Fig. S5C) of the lignin removal data revealed that lignin removal is closely related to the ultrasonication time, with a positive correlation of 0.961 and slightly related to the ultrasonication amplitude, with a positive correlation of 0.283. The PCA also revealed that DES soaking time did not affect the lignin removal with a correlation value of nearly 0. After removing the lignin fraction, the extracted yield of CMC was evaluated as 44.12 ± 2.17 % (w/w). This yield was later examined to include ~11 % of associated hemicellulose, which was removed during the CNC production process. Apart from eliminating lignin, there was an additional 6 % (*w*/w) solvent washing loss, ascribed to ultrasonic-lysed water-soluble biomass.

The extracted CMC was further subjected to CNCs extraction through glycerol soaking, followed by ultrasonication. The CCD related to the average particle size distribution of CNCs is tabulated in Table S3. The least average particle size of extracted CNCs was estimated to be 74.17 ± 9.73 nm, but this was obtained at a very high ultrasonication time of 35 min. Therefore, the trial with a significant particle size difference with the least sonication time was selected from the CCD (36 h glycerol soaking time with ultrasonication operating amplitude and time of 80 % and 15 min, respectively). The PCA correlation plot (Fig. S6 A), mono-plot (Fig. S6B), and bi-plot (Fig. S6C) of the CNCs conversion data revealed that the average particle size of the CNCs heavily depended on the ultrasonication time and ultrasonication amplitude, with corresponding correlation values of −0.668 and − 0.432. The negative nature of the value relies on the reduction of the average particle size. The glycerol soaking time moderately influences the particle size reduction of CNCs. The bi-plot of the PCA reveals that the selected component axes, PC1 and PC2 represent 46 % and 29.5 % of the nanocellulose conversion data, denoting the effective arrangement of the four-dimensional data in the 2D plot. The yield of CNCs from CWs was estimated to be 32.58 ± 2.76 % (*w*/w), with nearly 10 % (w/w) solvent washing. This loss can be ascribed to the removal of amorphous hemicellulose components from the crystalline backbone of cellulose.

3.1.1. Advantages of the proposed process compared to the other methods of extraction

The most conventional method of pectin extraction is acid-based (pH —1-2.5), high-temperature-mediated (70–100 °C) extraction with a solid to solvent ratio between 10 and 40 *w/v* operating for 30 to 120 mins. (Panwar et al., 2024) achieved a pectin yield of 22.20 % (*w*/w) with the conventional method from *citrus limetta* peels. (Siddiqui et al., 2021) achieved a pectin yield of 25–38 % (w/w) from the sweet lime peel with the ultrasonication-assisted extraction method with a solvent-to-solid ratio of (18:1 to 30:1), operating at the intensity of 48 to 80 % amplitude for 15–35 min. (Rahmani et al., 2020) achieved a pectin yield of 25.31 % (w/w) from the sweet lemon peel with an acid-based (pH -1.5 to 3.25) microwave-assisted extraction method with a solvent-to-solid ratio of 18:1 to 30:1, operating at 700 W power for 3 min. (Chiang & Lai, 2019; Liew et al., 2016) Chiang achieved 6.84 % (w/w) of pectin mucilage extraction from *Asplenium australasicum* and Liew achieved 7.12 % (w/w) of pectin extraction from passion fruit peel using an enzyme-assisted extraction method. Recently, supercritical solvent, subcritical solvent and plasma extraction methods have gained more attention among researchers. Among these recent extraction methods, supercritical and plasma extraction methods are mainly employed to extract bioactive. (Liew et al., 2018) employed the subcritical water extraction method and achieved 19 % (w/w) pectin yield from *Citrus grandis* peel. All the above-mentioned recent extraction techniques only focus on the extraction of pectin from the peels and don't give an overall process technology for the complete valorisation of the wastes. The main advantage of the process proposed in our work is the series of ultrasonication-based procedures for completely valorising the citrus wastes. To the best of our knowledge, (Al Jitan et al., 2022) have only reported the extraction of cellulose from citrus waste till now, and a sequential procedure for the extraction of extractives, pectin and nano cellulose from citrus waste has not been reported elsewhere. The chemical composition mass balance of the dried CW with the corresponding extraction yield achieved in the proposed ultrasonication process is tabulated in Table S6. We have achieved >90 % extraction efficiency for extractives, pectin and nano cellulose from citrus wastes with the possible recovery of hemicellulose and other compounds from washing solvents for further utilisation as feedstock in microbial production of biomolecules.

3.1.2. Scalability of the proposed process

Except for hexane, which is used to extract non-polar components in CW, All the solvents used to extract pectin, cellulose, and polar bioactive are eco-friendly. Thus, the proposed process is easily scalable; we have scaled up the process from 100 g to 500 g with the proposed process. The pilot scale trials are required to scale up the process further. The extraction of polar and non-polar components can also be investigated using supercritical solvents to avoid the usage of hexane in the given process. After the pilot scale trials, the proposed process will be transferred to our industrial partners.

3.1.2.1. Chemical characterisation of polar and non-polar CEs. The polar and non-polar CEs were analysed for their chemical constituents by liquid chromatography/mass spectrometry. The chemical constituents of polar and non-polar CEs are tabulated in Tables S7 and S8, respectively. The citrus peels are rich in aromatic phenolic compounds, such as terpenes, limonene (Lubinska-Szczygeł et al., 2018), and fatty acids such as stearic acid, linoleic acid, and linolic acid (Matsuo et al., 2019). The polar CEs of CWs were examined to be rich in hesperidin (17.13 ± 2.54 %), sucrose (16.95 ± 1.75 %), narirutin (9.70 ± 1.16 %), citric acid (7.76 ± 1.28 %), linoleic acid (4.21 ± 1.55 %) and trace amounts of other compounds. The major constituent hesperidin is a flavonoid having high antioxidant, anti-inflammatory, and anticancer activities (Iranshahi et al., 2015; Kırcı et al., 2023). The concentrated hydrophobic liquids present in plant cells are called essential oils. The citrus peel is a valuable raw material for essential oil extraction. It is composed of volatile aromatic chemicals and makes about 0.5–5 % of the fresh weight of citrus peel (Singh et al., 2021). The extraction of essential oils

from citrus fruit manufacturing wastes drew the attention of several researchers. Steam distillation (Chen et al., 2016), solvent extraction (Teigiserova et al., 2021), mechanical expression (Yi et al., 2018), microwave (Chen et al., 2016), and critical fluid (Menichini et al., 2011) extraction are some of the techniques used to extract essential oils. The primary constituent in the essential oils of many citrus species has been reported to be the colourless aliphatic hydrocarbon limonene (Singh et al., 2021). It is a nonoxygenated cyclic monoterpene and is made up of two isoprene units. It is also frequently used as a flavouring component in popular foods and is well-known for its pleasant citrus scent. In our work, CWs were examined only to have traces of limonene; this is due to the mechanical extraction of citrus flavours from the peels in the industry. The non-polar CEs of CWs were examined to be rich in triglycerides of 18 carbon and 16 carbon fatty acids, namely TG 54:6 (7.40 ± 1.26 %), TG 52:4 (7.18 ± 1.13 %), TG 54:5 (5.64 ± 1.29 %), TG 54:7 (4.53 ± 1.22 %), TG 54:3 (3.49 ± 1.12 %), and trace amounts of other triglycerides and free fatty acids.

3.2. Characterisation of CP, CMC, and CNCs

3.2.1. Physical characterisation

The particle size of polymers generally represents the compactness and structural integrity of the molecule, and it depends on the source of the polymer, molecular mass and intra-molecular interactions between monomers (Rivadeneira et al., 2020; Zhuang et al., 2019). The particle size and morphology of macromolecules such as pectin and cellulose affect their rheological properties; low particle size molecules tend to have better flow properties and dispersity in water to give good colloidal solutions (Dogan et al., 2018). The CP and CMC molecules extracted from CWs were estimated to have an average particle size of 889 nm, and 640 nm (Fig. 1A), respectively. The observed particle size distribution of CP is higher than the pectin extracted from banana peel (Rivadeneira et al., 2020), and comparable to the pomegranate peel pectin (Zhuang et al., 2019). The large average particle size of extracted CP can be ascribed to its high average molecular weight (167.1 kDa) observed in HP-SEC analysis (Fig. 1C). The molecular weight of CMC was estimated to be 109.5 kDa. The average particle size of CNCs converted from CMC was found to be 175 nm with an average molecular weight of 55.3 kDa. This reduced average particle size and molecular weight of CNCs can be attributed to the effectiveness of the high amplitude ultrasonic disruption of the amorphous cellulose region (W. Chen et al., 2011;Harini et al., 2018 ; Harini & Chandra Mohan, 2020). The DLS particle size measurement can only give the approximate particle size values of the cellulose crystals, and it cannot give the exact diameter measurement. This can be attributed to the linear nature of cellulose fibres. DLS particle size measurements mainly depend on the scattering of light from colloidal sphere suspensions. Therefore, the particle size of linear cellulose fibres cannot be measured through the DLS method, thus it can only be used for fast shortlisting of the process. Similar observations were also noted and explained by (Gong et al., 2017) and in our previous studies (Harini et al., 2018; Harini & Chandra Mohan, 2020). The ζ-potential of the biological polysaccharides should be above ±30 mV to have a stable dispersion in water (Chu et al., 2020; Prathapan et al., 2016). The ζ-potential (Fig. 1B) of CP and CMC was estimated to be −37.60 mV and − 27.87 mV, respectively. These results imply that extracted CP can produce stable dispersions with water, but CMC can produce only agglomerated dispersions. The ζ-potential of CNCs (−48.13 mV) was significantly different ($P < 0.05$) compared to CMC, forming a stable dispersion in water. The XRD spectra (Fig. 1D) of CP did not show sharp crystalline peaks. This may be ascribed to the branched, amorphous nature of CP (Du et al., 2023). The CMC and CNCs showed distinct crystalline peaks around 22.52°, ascribed to the 002 crystal structure of cellulose (Harini et al., 2018; Harini & Chandra Mohan, 2020; Wulandari et al., 2016). The intensity of the crystalline peak of CNCs at 22.52° was observed to be higher than the CMC crystalline peak due to the high crystalline nature of CNCs compared to CMC, which was due to the effective removal of the amorphous regions during the CMC-to-CNCs conversion process by ultrasonication. The crystallinity index of CNCs and CMC were evaluated to be 87.85, and 62.16 %, respectively.

Fig. 2 illustrates the thermal degradation properties of the extracted polysaccharides. The TG traces reported in Fig. 2A show different patterns of mass loss for CP, CMC, and CNCs, revealing that the CMC sample has the greatest resistance against thermal degradation, whereas CNCs

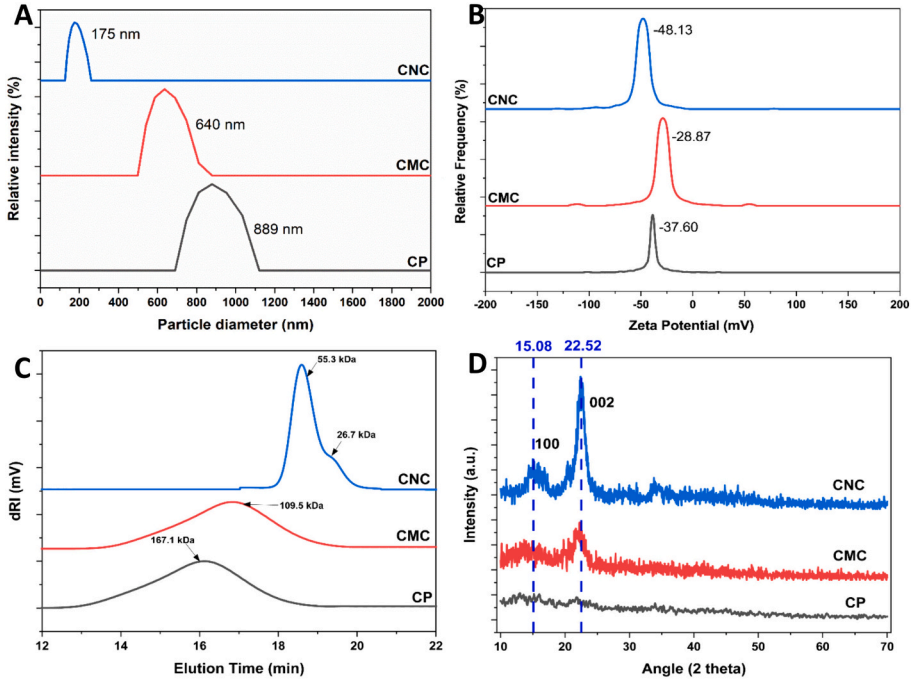

Fig. 1. A - Particle size of CP, CMC, and CNC; B - ζ-potential of CP, CMC, and CNC; C - molecular weight of CP, CMC, and CNC; D – X-ray diffraction of CP, CMC, and CNC [CP – Citrus Pectin; CMC – Citrus Microcellulose; CNC – Citrus Nanocellulose].

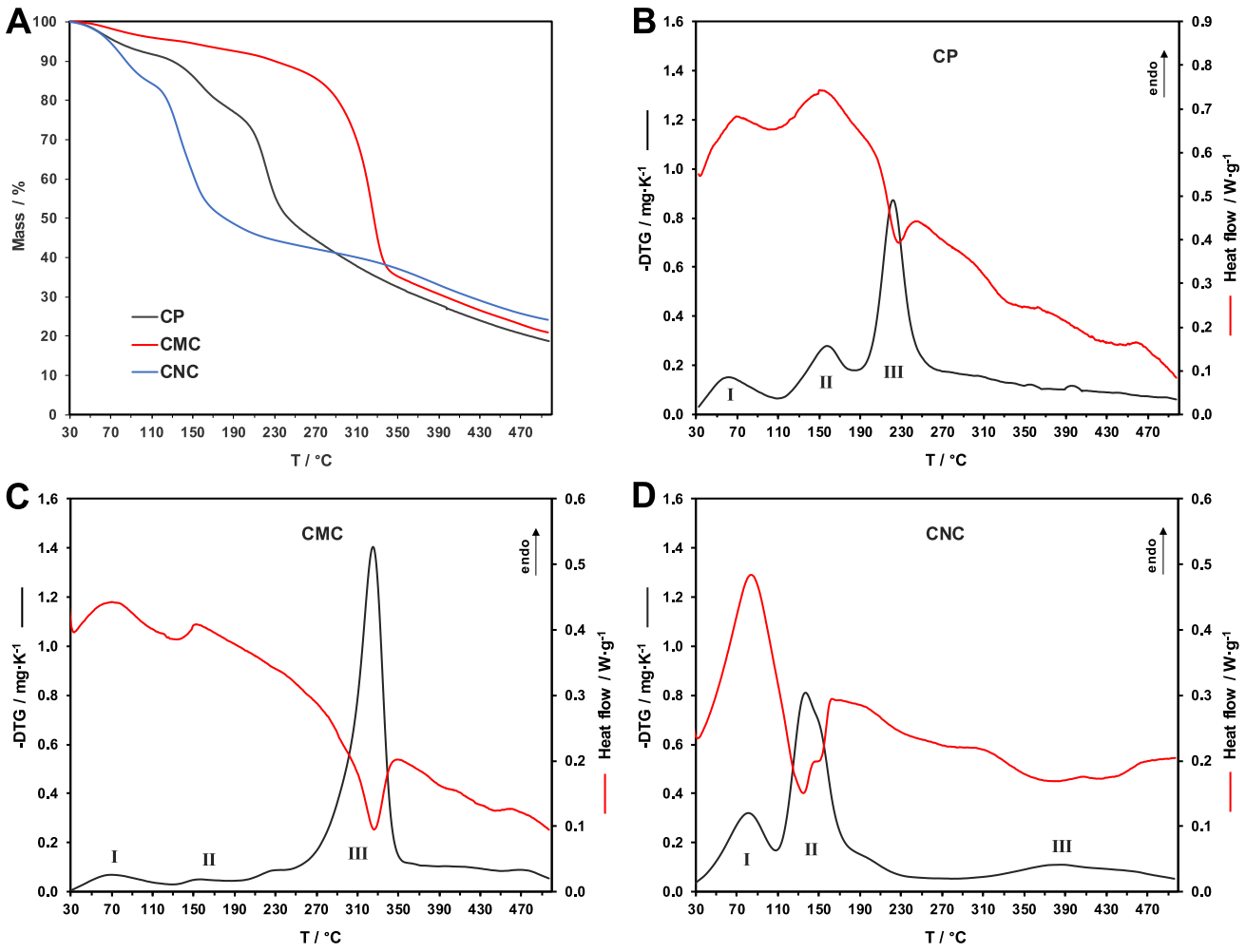

Fig. 2. A – Thermogravimetry of CP, CMC, and CNC; B – DTG and DSC thermogram of CP; C – DTG and DSC thermogram of CMC; D – DTG and DSC thermogram of CNC [CP – Citrus Pectin; CMC – Citrus Microcellulose; CNC – Citrus Nanocellulose].

exhibits earlier degradation phenomena upon temperature rise. In any case, the residual mass at 500 °C is quite similar among the three polysaccharides and correspond to about 19 %, 21 %, and 24 % for CP, CMC, and CNCs, respectively.

To better discriminate the phenomena lying under the mass loss across the temperature range considered, Fig. 2B, C and D report the temperature derivative (DTG) of the three TG traces shown in panel A, as well as the thermal effects involved in the process.

Concerning CP, the DTG trace in Fig. 2B shows three prominent peaks corresponding to three main events, which clearly involve mass loss due to thermal effects. Going into more detail, DTG peaks I and II are associated with two endothermic events that can be ascribed to diffusional and bound water loss, respectively. Similar regions (up to 190 °C) are also observed in the literature for CP's water loss (W. Wang et al., 2016; Wani & Uppaluri, 2023). Instead, peak III, which is associated with the greatest CP mass loss and shows a maximum at about 222 °C, reflects the pyrolytic decomposition of the polysaccharide, as confirmed by the exothermic event recorded in the heat flow trace between 190 °C and 260 °C. According to the literature, the galacturonic acid chains start to undergo thermal degradation during this interval, leading to the evolution of several gaseous products (due to decarboxylation) and to the formation of solid char (Einhorn-Stoll et al., 2007; W. Wang et al., 2016). The latest part of the DTG trace (above 260 °C) shows a slower mass loss ascribable to further thermal degradation of the remaining char, as confirmed by the small exothermic contributions exhibited by the heat flow trace.

Analogously to CP, CMC also exhibits a multi-stage thermal degradation behaviour with three main mass loss events. Although less marked than CP's, CMC's peaks I and II are ascribable to diffusional and bound water loss, as already observed in the literature for orange peel cellulose crystals with a similar size distribution (L. Chen et al., 2024). Peak III is again associated with the pyrolytic degradation of the polysaccharide, as revealed by the exothermic event recorded by the DSC trace and occurring through the breakdown of the glucosidic structure, aromatisation and formation of carbonyl compounds (Lichtenstein & Lavoine, 2017). Across peak III interval, i.e., from 210 °C to 350 °C with a peak maximum of about 325 °C, CMC undergoes a weight loss of about 50 %, and then a slower decomposition process of the pyrolysis residue continues.

Finally, CNCs share peak I with CMC, which is attributable to diffusional water loss. However, the loss of bound water within the peak II region appears to overlap with a more extended and anticipated mass drop due to the thermal degradation of cellulose chains as the observable overall exothermic effect reveals (peak maximum at about 147 °C). The peak appears broader and shouldered, indicating a distribution of CNC particles with different stabilities that may be correlated with the two main CNC size populations already described in Fig. 1C. A third mass loss peak is also visible at higher temperatures and may again be associated to a pyrolytic degradation of the polysaccharide, as revealed by the exothermic event recorded by the DSC. Comparing CNCs with the CMC behaviour, we may argue that the degradation processes are of the same nature, but the main CNCs degradation event (corresponding to a

weight loss of about 35 %) is clearly anticipated, indicating a less stable system. Similar early degradation for CNCs is also reported by Phanthong et al. (2015), though in the case of materials that underwent hydrolysis (Phanthong et al., 2015). In any case, literature reports that CNCs often exhibit lower stability than CMC depending on the extraction process (Onkarappa et al., 2020) and natural source (Harini & Chandra Mohan, 2020).

Fig. 3 illustrates the macro structures of CP, CMC, and CNCs. The extracted CP was observed to be a coarse powder with irregularly shaped amorphous solids. Dogan et al. (2018) studied the morphology of various hydrocolloids and reported that pectin is an irregularly shaped macromolecule. Wang et al. (2017) reported that pectin is an irregular amorphous solid in powder form, while forming interconnecting networks with hydrogen bonds to give fibrous layers when it is dissolved in water. CMC was observed to be a linear bundle of crystalline cellulose fibres stacked above one another and connected by amorphous hemicellulose layers. Anari et al. (2024) worked on the extraction of cellulose from walnut shells with DBD plasma and reported a similar influence of hemicellulose and lignin in microcellulose structure. In our work, we effectively separated the CEs and lignin from the native citrus cellulose using DES-assisted ultrasonic treatment. CNCs appeared to be crystalline needle-like whiskers, evidencing the effective removal of amorphous hemicellulose connecting layers from the backbone of crystalline cellulose. This size reduction and removal of amorphous regions of cellulose can be ascribed to the effective ultrasonic disruption of these regions (Chen et al., 2011; Cheng et al., 2009; Harini et al., 2018; Harini & Chandra Mohan, 2020). The size and macro-morphology of CNCs were measured further with AFM. The height parameters of the AFM surfaces were analysed using the ISO 25178 method, and the average width of the nanocrystals was found to be 56.3 nm with an average aspect ratio of 1.96, respectively. This parameter falls within the definition of cellulose nanocrystals described by other researchers (Cellulose Nanocrystals (CNC or NCC): These are rigid rod-shaped monocrystalline cellulose domains (whiskers) with diameters ranging from 1 to 100 nm and lengths spanning from tens to hundreds of nanometers (Bai et al., 2009; Thomas et al., 2020; Trache et al., 2020)). This overall height profile of AFM within 100 nm proves the effectiveness of the ultrasonication treatment in CNCs production.

3.2.2. Chemical characterisation

FTIR spectra of polysaccharides extracted from CWs are shown in Fig. 3A, and their band assignments are tabulated in Table 1. CP showed its characteristic peaks of O—H stretching (3287 cm^{-1}), C—H stretching (2918 cm^{-1}), C═O stretching (1645 cm^{-1}), C-O-C glycosidic stretching (~1100–1000 cm^{-1}), and sugar ring skeletal vibrations (1148, 1104, and 939 cm^{-1}). Other researchers observed and reported similar band assignments (Qi et al., 2023; Wang et al., 2023; Xia et al., 2020). The galacturonic acid content (GAC) of pectin can be estimated using the FTIR carbonyl peak area correlation (Monsoor et al., 2001), whereas the esterification degree (DE) of pectin can be calculated by correlating the FTIR ester (~1700 cm–1) and carbonyl peak area (Yu et al., 2021). In this work, the GAC and DE of extracted CP were estimated to be 61.81 %. and 59.92 %, respectively. CMC showed its characteristics peak of O—H stretching (3343 cm^{-1}), C—H stretching (2922 cm^{-1}), C═O stretching (1632 cm^{-1}), C-O-C glycosidic stretching (~1100–1000 cm^{-1}), and sugar ring skeletal vibrations (1148, 1104, and 939 cm^{-1}). CNC showed its characteristics peaks of O—H stretching (3335 cm^{-1}), C—H stretching (2929 cm^{-1}), C═O stretching (1731 cm^{-1}), C-O-C glycosidic stretching (~1100–1000 cm^{-1}), and sugar ring skeletal vibrations (1148, 1104, and 939 cm^{-1}). Other researchers observed and reported similar band assignments for micro and nanocellulose (Javier-Astete et al., 2021; Md Salim et al., 2021). The crystallinity index of cellulose can be measured by calculating the difference in peak areas of 1430 cm^{-1} and 898 cm^{-1} (Karimi & Taherzadeh, 2016). The crystallinity index calculated from FTIR analysis of CMC and CNCs was estimated to be 47.88 and 70.37 %, respectively.

The ^{13}C NMR chemical shift frequencies of polysaccharides extracted from CWs are illustrated in Fig. 4B, and their resonance frequency assignments are tabulated in Table 1. The characteristic chemical shifts of C^1 (101.57), C ^{2,3,5} (73.59–65.27), C^4 (80.30), C^6 (53.98), $COOCH_3$ (171.68), and $OCOCH_3$ (17.86) were observed for extracted CP. Similar chemical shift frequencies were noted for pectins extracted from sweet potatoes (Nurdjanah et al., 2013), *Adansonia digitata* (Patova et al., 2021) and *Punica granatum* (Shakhmatov et al., 2019, 2020). The GAC of pectin can be estimated by calculating the difference between the peak area of C^6 and the average peak area of C^{1-6} (Nurdjanah et al., 2013; Zhu et al., 2014). The esterification degree of pectin can be estimated by calculating the difference between the peak area of $COOCH_3$ and the

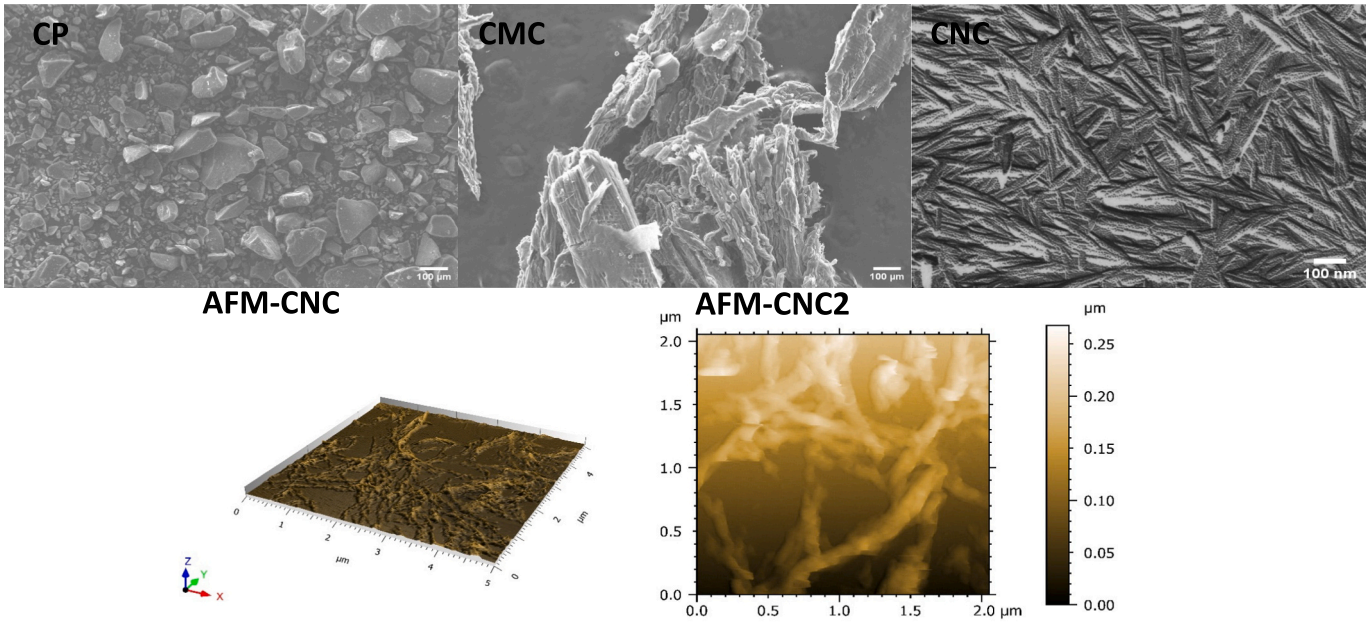

Fig. 3. Morphology of CP, CMC and CNC – (CP - SEM images of citrus pectin; CMC – SEM image of citrus microcellulose; CNC – SEM image of citrus nanocellulose; AFM-CNC - 3D AFM image of citrus nanocellulose; AFM-CNC2 - 2D AFM image of citrus nanocellulose].

Table 1
NMR frequency and FTIR band assignments of CP, CMC, and CNC.

NMR resonance assignments and corresponding GAC, DE, and crystallinity calculations						
Samples	C_1	$C_{2,3,5}$	C_4	C_6	$COOCH_3$	$OCOCH_3$
^{13}C chemical shift frequency (ppm)						
CP	101.57	73.59–65.27	80.30	53.98	171.68	17.86
CMC	101.11	77.65–67.62	~79.80–92.11	64.01	nd	nd
CNC	100.87	77.90–67.37	~79.80–92.11	63.80	nd	nd
Galacturonic acid content of CP (GAC)		54.64 %		**Crystallinity index of CMC**		52.34 %
Degree of Esterification of CP (DE)		40.66 %		**Crystallinity index of CNC**		78.67 %

FTIR Band Assignments and corresponding GAC, DE, and Crystallinity calculations								
Samples	O-H stretching vibrations	C-H stretching vibration	Ester/Carbonyl C═O stretching vibration	O-H in plane bending	C-H bending/CH_2 wagging	C-O stretching	Glycosidic C-O-C linkage stretching vibrations	Sugar ring skeletal stretching vibrations
Wave numbers (cm^{-1})								
CP	3287	2918	1701, 1645	1458	~1300–1380	1240	~1100–1000, 890	1148, 1104, 939
CMC	3343	2922	1701, 1632	1447	~1300–1380	1240	~1100–1000, 890	1148, 1104, 939
CNC	3335	2929	1731	1447	~1300–1380	1240	~1100–1000, 890	1148, 1104, 939
Galacturonic acid content of CP (GAC)		61.81 %		**Crystallinity index of CMC**		47.88 %		
Degree of Esterification of CP (DE)		59.92 %		**Crystallinity index of CNC**		70.37 %		

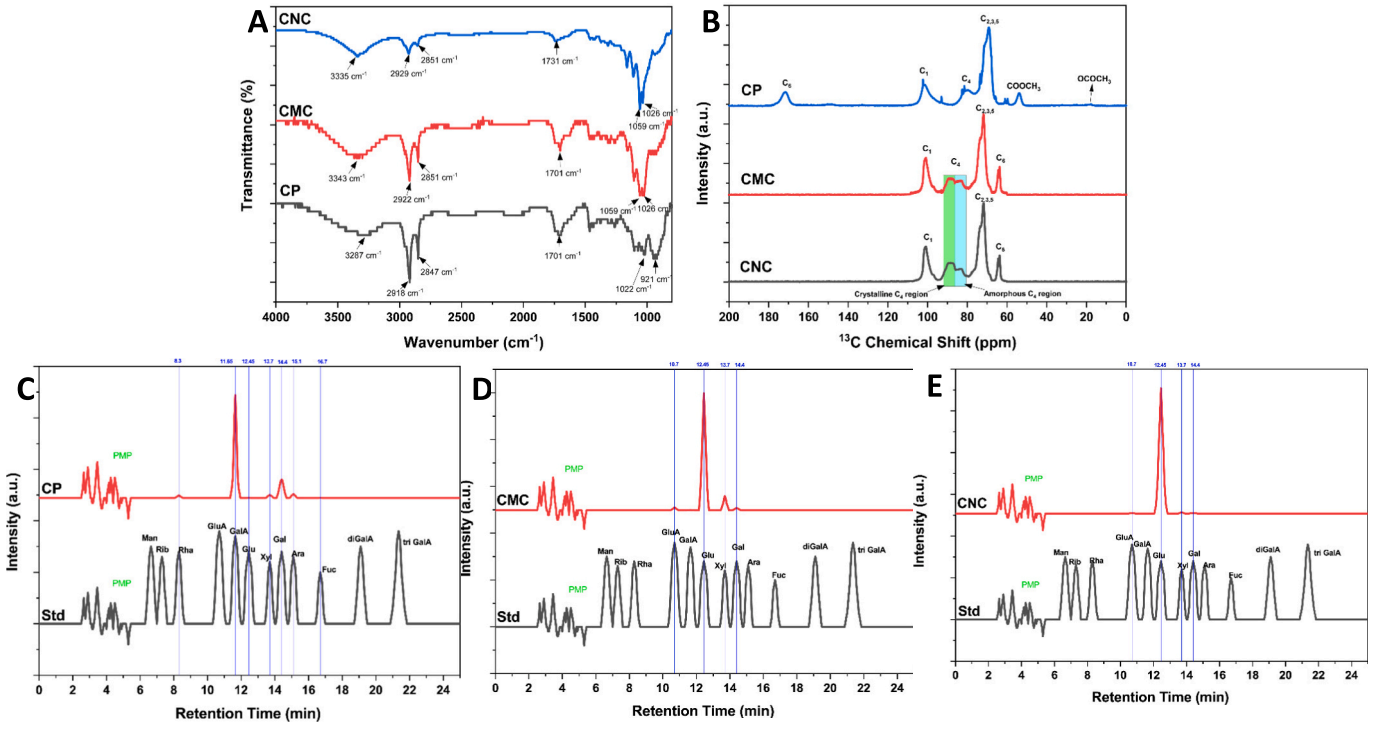

Fig. 4. Chemical characterisation of CP, CMC, and CNCs (A – FTIR spectra; B – CP-MAS NMR spectra; C – HPLC chromatogram of hydrolysed CP; D – HPLC chromatogram of hydrolysed CMC; E – HPLC chromatogram of hydrolysed citrus CNCs) [CP – Citrus Pectin; CMC – Citrus Microcellulose; CNC – Citrus Nanocellulose; Std – Standard sugars; PMP - 1-phenyl-3-methyl-5-pyrazolone].

average peak area of C^{1-6} (Nurdjanah et al., 2013; Zhu et al., 2014). The GAC and DE of CP were estimated to be 54.64, and 40.66 % by NMR spectral analysis. The micro and nanocellulose extracted from CWs showed characteristic chemical shifts of 101.11/100.87 ppm (C^1), 77.65–67.62/77.90–67.37 ppm ($C^{2,3,5}$), ~79.80–92.11 (C^4), and 64.01/63.80 (C^6), respectively. Similar chemical shift assignments were observed for cellulose extracted from orange bagasse (M. A. Mariño et al., 2018), corncob (Rovera et al., 2023) and banana peel (Harini et al., 2018). The crystallinity index of cellulose can be estimated by calculating the difference between the crystalline C^4 peak area and the total C^4 peak area (Rovera et al., 2023). The crystallinity index of CMC and CNCs was estimated to be 52.34, and 78.67 % through NMR

analysis, respectively. In both FTIR and NMR-derived crystallinity indexes, the crystallinity of CNCs was examined to be higher than CMCs. This can be ascribed to the fact that high-amplitude ultrasonication breaks the amorphous regions of cellulose to produce highly crystalline nanocellulose (Harini et al., 2018; Harini & Chandra Mohan, 2020). It was also observed that the crystallinity index value evaluated by FTIR and NMR have a ~ 10 % difference. This difference can be ascribed to the nature of this analytical method, which can only give the relative crystallinity of the materials (Karimi & Taherzadeh, 2016).

The monosaccharide composition of the polysaccharides extracted from CWs was analysed through acid hydrolysis followed by PMP-derived HPLC analysis. The HPLC chromatograms of CP, CMC, and CNCs are illustrated in Fig. 4C, D, and E, respectively. The hydrolysed samples were compared with monosaccharide standards to evaluate the composition of the polysaccharides both qualitatively and quantitatively. The quantitative and qualitative monosaccharide composition of the CP, CMC, and CNCs are tabulated in Table 2. CP was examined to be rich in galacturonic acid and galactose. The high amount of galacturonic acid can be ascribed to the linear polygalacturonic nature of CP. Other monosaccharides such as galactose, arabinose, glucose, rhamnose, xylose, and fucose can be attributed to rhamnogalacturonan 1 and rhamnogalacturonan 2 fraction of CP. Moreover, xylose may also be attributed to the xylogalacturonan fraction of CP. The monosaccharide composition of CMC was examined to be rich in glucose, which can be attributed to the anhydrous glucose backbone structure of cellulose. It was also found to have a small amount of xylose and trace amounts of glucuronic acid, galacturonic acid, and galactose. Xylose is the primary monosaccharide of hemicellulose, constituting xylan (Rao et al., 2023). Thus, the presence of xylose with trace amounts of other monosaccharides may be ascribed to the amorphous hemicellulose layer connecting the crystalline cellulose backbone. CNCs extracted from CWs were found to be rich in glucose and trace amounts of other monosaccharides. This can be attributed to the high crystalline linear arrangement of glucose units in CNCs, also evidenced through the crystallinity index values observed in XRD, FTIR, and NMR analyses.

3.2.3. *Structural characterisation*

Polysaccharides are complex molecules, which require in-depth characterisation techniques for elucidating their structure. The structure of cellulose is well documented and it consists of the linear arrangement of glucose units by (1 → 4) β-glycosidic linkages. The structure of CMC and CNCs extracted from CWs, which were found to be rich in glucose with high crystallinity index and characteristic NMR/FTIR spectral patterns, were termed to have linear Glu (1 → 4) β-Glu pattern of holo- or alpha-cellulose and residual amorphous hemicellulose consists of xylan as a significant constituent (Rao et al., 2023). Meanwhile, CP extracted from CWs is examined as a more complexly branched polymer of interest in this study. The structure of CP was elucidated by enzymatic treatment of CP with three different enzymes, namely *endo*-PG, rhamnogalacturonan lyase, and *exo*-PG. The various fractions of the lysed CP were analysed for their monosaccharide compositions and fragmentation patterns. The resulting monosaccharide compositions were correlated with the ESI-MS fragmentation patterns to elucidate the putative structure of the CP. The endo-PG hydrolysed CP sample was collected periodically at 6, 12, and 18 h intervals. After PMP derivatisation, the collected samples were eluted through HPLC to analyse the monosaccharide fractions. The enzyme-hydrolysed fractions were collected separately and subjected to acid hydrolysis to examine their monosaccharide composition. The HPLC chromatogram of endo-PG hydrolysed CP is illustrated in Fig. 5. The CP hydrolysed for 6 h with endo-PG showed various elution fractions, with primary monosaccharide composition of galacturonic acid and di, tri, and other oligomeric fractions of galacturonic acid. The presence of these oligomeric fractions may be attributed to the hydrolysis of the polygalacturonic acid backbone of CP. The xylogalacturonic acid oligomer fraction was also observed in the endo-PG hydrolysed CP, attributed to the xylogalacturonan section of the CP structure. After 18 h of endo-PG hydrolysis, apart from mono-, di-, tri-galacturonic acid, and xylogalacturonan (ascribing to HG fraction), significant fractions at the retention time of 38.16 and 33.48 min were observed, attributed to the RG-I, and RG-II, respectively. The monosaccharide compositions of the HG, RG-I, and RG-II fractions of CP were tabulated in Table 3. The HG fraction resulted to be rich in galacturonic acid and traces of xylose, galactose, and arabinose. The RG-I fraction was rich in galactose, galacturonic acid, arabinose, and rhamnose. The RG-II fraction was examined to be rich in galactose, galacturonic acid, fucose, arabinose, rhamnose, glucose, and xylose. The structure of the HG fraction of CP is well documented, and complete enzymatic hydrolysis of the HG fraction reveals the linear arrangement of galacturonic acid with (1 → 4) α-glycosidic linkages. The traces of xylose, galactose, and arabinose in the HG fraction can be attributed to mono and disaccharide side chains attached to the HG fractions to give xylogalacturonan part of the CP structure.

The structural elucidation of RG-I and RG-II fractions of CP is more complicated due to the complexity of branches with multiple monomers. Thus, CP's RG-I and RG-II fractions were separated and subjected to consecutive enzymatic hydrolysis with rhamnogalacturonan lyase and exo-PG. The resultant solutions were eluted through HPLC, and their

Table 2
Monosaccharide composition of extracted CP, CMC, and CNCs.

Monosaccharides	Short form	CP	CMC	CNCs
		Composition in mol%		
Mannose	Man	nd	nd	nd
Ribose	Rib	nd	nd	nd
Rhamnose	Rha	1.8 ± 0.57	nd	nd
Glucuronic acid	GluA	nd	1.8 ± 0.12	0.30 ± 0.07
Galacturonic acid	GalA	79.20 ± 3.56	0.20 ± 0.08	nd
Glucose	Glu	0.20 ± 0.07	86.40 ± 2.15	98.50 ± 1.37
Xylose	Xyl	1.90 ± 0.73	10.20 ± 1.74	0.90 ± 0.15
Galactose	Gal	13.90 ± 1.86	1.40 ± 0.18	0.30 ± 0.11
Arabinose	Ara	2.90 ± 1.05	nd	nd
Fucose	Fuc	0.10 ± 0.03	nd	nd

Results are represented in the form of Mean ± S.E.
nd – Not Detected

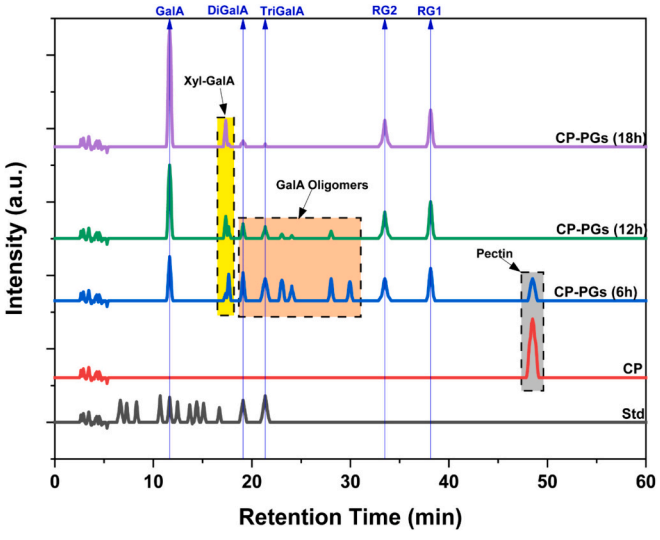

Fig. 5. HPLC chromatograms of endo-PG hydrolysed CP. [CP – Citrus Pectin; CP-PGs (6 h) – Citrus pectin hydrolysed with Endo-PG for 6 h; CP-PGs (12*h*) – Citrus Pectin hydrolysed with Endo-PG for 12 h; CP-PGs (18 h) – Citrus Pectin hydrolysed with Endo-PG for 18 h; Std – Standard sugars; GalA: Galacturonic acid; DiGalA – di-galacturonic acid; TriGalA – tri-galacturonic acid; Xyl – Xylose; RG1 – Rhamnogalacturonan I fraction; RG2 – Rhamnogalacturonan II fraction; PMP - 1-phenyl-3-methyl-5-pyrazolone].

Table 3
Monosaccharide composition of endo-PG hydrolysed fractions from extracted CP.

Monosaccharides	Short form	HG	RG-I	RG-II
		Composition in mol%		
Mannose	Man	nd	nd	nd
Ribose	Rib	nd	nd	nd
Rhamnose	Rha	nd	10.34 ± 1.27	10.23 ± 1.15
Glucuronic acid	GluA	nd	nd	nd
Galacturonic acid	GalA	96.34 ± 2.17	27.87 ± 2.49	19.74 ± 2.78
Glucose	Glu	nd	nd	5.22 ± 1.15
Xylose	Xyl	1.14 ± 1.03	nd	4.98 ± 1.54
Galactose	Gal	1.43 ± 0.08	40.51 ± 2.94	25 0.83 ± 3.42
Arabinose	Ara	1.09 ± 0.13	21.28 ± 1.68	12.57 ± 1.63
Fucose	Fuc	nd	nd	21.43 ± 1.83

Results are represented in the form of mean ± S.E.
nd – Not Detected.

chromatograms are depicted in Fig. S7A&B. The RG-I fraction was observed to be separated into three fractions, with the release of rhamnose and galacturonic acid monomers. The RG-II fraction was observed to be divided into two fractions, with the release of galacturonic acid. These separated fractions were further analysed for their monosaccharide composition through acid hydrolysis and PMP-assisted HPLC analysis. The HPLC chromatogram of the hydrolysed RG-I fractions 1, 2, and 3 are illustrated in Fig. S7C. The monosaccharide compositions of these fractions are tabulated in Table 4. The RG-I fraction 1 and fraction 2 were examined to be rich in arabinose and galactose, respectively. The RG-I fraction 3 was examined to be rich in arabinose and galactose at the molar ratio of 1:2. The HPLC chromatogram of hydrolysed RG-II fractions 1 and 2 are illustrated in Fig. S7D. The monosaccharide compositions of these fractions are tabulated in Table 4. The RG-II fraction 1 was examined to be rich in arabinose and fucose at the molar ratio of 1:3. The RG-II fraction 2 was examined to be a complex polymeric side chain with major monomers of galactose, fucose and rhamnose, with traces of glucose, xylose, and arabinose.

The different fractions of RG-I and RG-II were subjected to ESI-mass spectroscopy analysis to predict their structural makeup. The structural predictions of the RG fractions relied on the examined molar ratio of monosaccharides and previously reported fragmentation patterns of different oligomers of arabinose (Juvonen et al., 2019; Kouzounis et al., 2022; Shi et al., 2020a; Tsai et al., 2021; Westphal et al., 2010), galactose (Lin et al., 2022; Logtenberg et al., 2020; Yan et al., 2024), the *Z*-ion dominance rule, and cross-ring cleavage ions. According to the fragmentation patterns noted by (Lin et al., 2022), cross-ring cleavage ions alone cannot provide sufficient features to differentiate between linear and branched structures. The Z-ion dominance represents that the intensity of Z-ion is substantially higher than its corresponding Y-ion. (Logtenberg et al., 2020) coined that this must be considered a distinctive feature for characterising branched polysaccharides. (C. C. Lin et al., 2022) investigated the Z-ion dominance rule for linear and branched polysaccharides and reported that the glycosidic cleavage and Z-ion dominance preferentially occurred at the side chain of the branch structures, while linear structures generate C/Y-ions other than B/Z-ions. These fragmentation patterns were used to confirm the linkage patterns between monosaccharides. The ESI-MS fragmentation pattern of RG-I fractions 1, 2, and 3 are illustrated in Fig. 6A, B, and C, respectively. The fragmentation pattern of RG-I fraction 1 showed an intense peak around 131.10 *m/z*, ascribed to the ionisation pattern of arabinose. Other intense peaks were also observed around 233.05, 365.11, 497.21, and 629.11 m/z, ascribed to ^{0,2} A-H_2O fragmentation pattern of the degree of polymerisation (DP) 2, 3, 4, and 5, respectively. This fragmentation pattern of RG-I fraction 1, in correlation with its monosaccharide composition, is elucidating the putative linear chain of 5 arabinose units linked with (1 → 5) α-glycosidic linkages. Similar fragmentation patterns were reported for oligomers of arabinose linked with (1 → 5) α-glycosidic linkages by (Shi et al., 2020a; Westphal et al., 2010). Thus, the RG-I fraction 1 of CP was elucidated to be an arabinan with DP5. The fragmentation pattern of RG-I fraction 2 showed an intense peak around 161.05 *m/z*, ascribing to the ionisation pattern of galactose. Peaks around 263.10, 425.15, 587.20, 749.19, 911.24, 1073.15, and 1235.21 m/z illustrate the ^{0,2} A-H_2O fragmentation pattern of the degree of polymerisation (DP) 2, 3, 4, 5, 6, 7, and 8, respectively. This fragmentation pattern of RG-I fraction 2, in correlation with its monosaccharide composition, is elucidating the putative linear chain of 8 galactose units linked with (1 → 4) β-glycosidic linkages. This linkage pattern was confirmed by previously reported galactooligomers' structure and fragmentation patterns (C. C. Lin et al., 2022; Yan et al., 2024). Thus, the RG-I fraction 2 of CP was elucidated to be a galactan with DP8. The fragmentation pattern of RG-I fraction 3 showed intense peaks around 131.12 and 161.05 *m/z*, corresponding to the ionisation pattern of arabinose and galactose, respectively. Intense fragmentation peaks around 263.10, 425.15, and 587.20 m/z elucidate the linear arrangement of four galactose units, after which fragmentation peaks around 719.17 and 749.19 m/z elucidates the attachment of arabinose as well as galactose, with 4th galactose unit. The fragmentation pattern of the arabinose side chain was observed from 719.17, 851.10, and 983.09 m/z, ascribed to the trisaccharide side chain constituting arabinose units. The linear fragmentation patterns of galactose with the side chain of trisaccharide arabinose unit were observed at 983.09, 1145.19, and 1307.08 m/z, ascribed to 4Gal(3Ara), 4Gal(3*Ara*)Gal, and 4Gal(3Ara)2Gal structural patterns, respectively. This fragmentation pattern of RG-I fraction 3, in correlation with its

Table 4
Monosaccharide composition of double enzyme hydrolysed RG fractions from extracted CP.

Monosaccharides	+	RG-I^			RG-II^	
		Fraction 1	Fraction 2	Fraction 3	Fraction 1	Fraction 2
		Composition in mol%				
Mannose	Man	nd	nd	nd	nd	nd
Ribose	Rib	nd	nd	nd	nd	nd
Rhamnose	Rha	nd	nd	nd	nd	17.87 ± 2.11
Glucuronic acid	GluA	nd	nd	nd	nd	nd
Galacturonic acid	GalA	nd	nd	nd	nd	nd
Glucose	Glu	nd	nd	nd	nd	8.84 ± 2.18
Xylose	Xyl	nd	nd	nd	nd	8.82 ± 1.03
Galactose	Gal	nd	100	66.67 ± 2.15	nd	36.76 ± 1.23
Arabinose	Ara	100	nd	33.34 ± 1.53	74.71 ± 2.57	8.92 ± 1.08
Fucose	Fuc	nd	nd	nd	25.29 ± 1.13	18.79 ± 1.57

Results are represented in the form of Mean ± S.E.
nd – Not Detected.

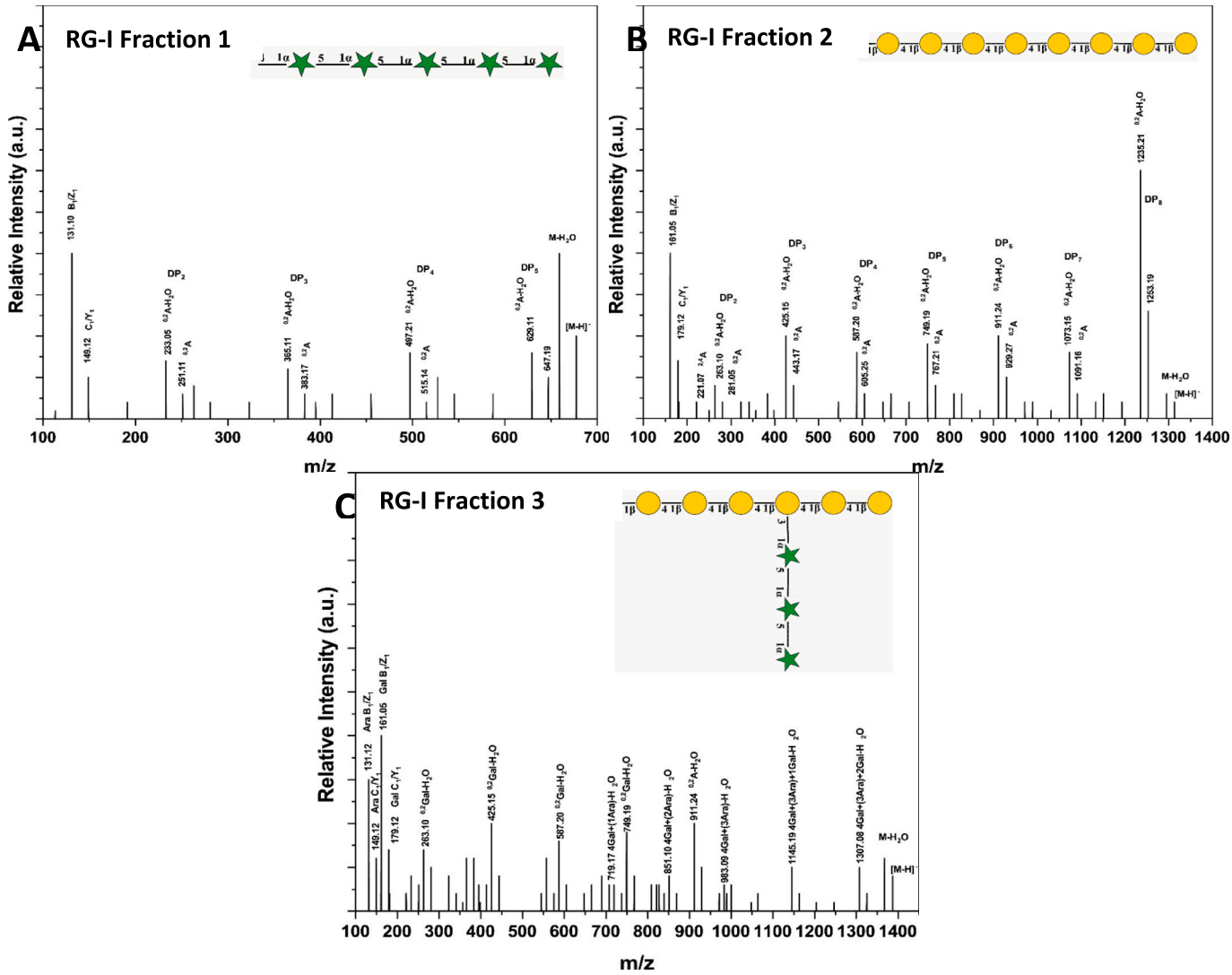

Fig. 6. ESI-Mass Spectra of RG-I Fractions [A – RG-I fraction 1; B – RG-I fraction 2; C – RG-I fraction 3].

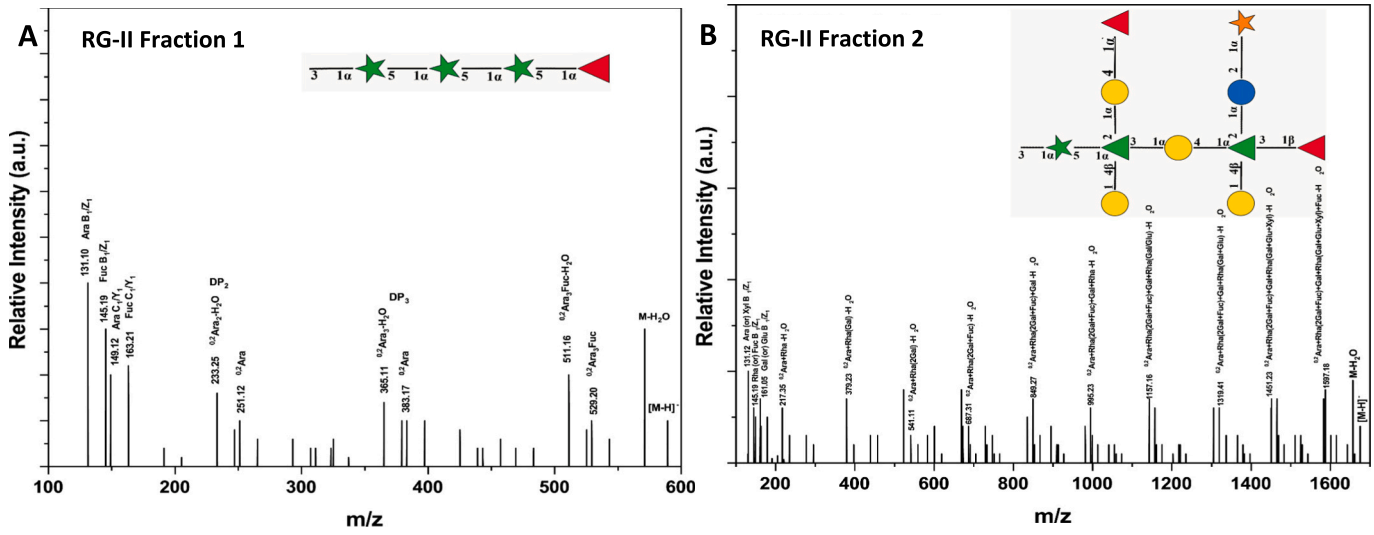

Fig. 7. ESI-Mass Spectra of RG-II Fractions [A – RG-II fraction 1; B – RG-II fraction 2].

monosaccharide composition, is elucidating the putative linear chain of 6 galactose units linked with (1 → 4) β-glycosidic linkages (Yan et al., 2024) and 3 arabinose units linked together by (1 → 5) α-glycosidic linkages (Shi et al., 2020b) connected with 4th galactose unit through (1 → 3) α-glycosidic linkage. This linkage pattern was observed from the dominance of Z1β over Y1β indicating four galactosyl units at the main chain and two at the extended linear chain of branched RG-I fraction. The occurrence of cross-ring cleavage on the penta-hexosyl units $^{0,4} \times _0$-H_2O excluded the possibility of 1 → 2;1 → 6 linkages; fragment $^{0,3}A_4$ and $^{0,2}A_4$-H2O (between tetra- to penta-galactosyl) excluded the possibility of 1 → 4;1 → 6 linkages. The remaining possible structure was 1 → 3;1 → 2 linkage of arabinose with fourth galactose on the main chain of 1 → 4 extension. The occurrence of ^{0,2} A-H_2O supported the structural illustration of a tri-arabinan side chain with 1 → 5 linkage from the non-reducing end. The lack of mono- to di-hexosyl characteristic fragments in between the 3rd and 5th galactose units supported the structural illustration of the 1 → 3 linkage between the 4th galactose in the main chain and the 3rd arabinose in the side chain (C. C. Lin et al., 2022). Thus, the RG-I fraction 3 of CP was elucidated to be a galacto-arabinan with DP9.

The ESI-MS fragmentation pattern of RG-II fractions 1 and 2 is illustrated in Figs. 7A and B, respectively. The RG-II fraction 1 showed intense peaks around 131.10 and 145.19 *m/z*, corresponding to the ionisation mass pattern of arabinose and fucose, respectively. The fragmentation peaks around 233.25, 365.11, and 511.16 m/z, indicate the linear arrangement of 2nd and 3rd arabinose units with terminal fucose units. In correlation with its monosaccharide composition, this fragmentation pattern elucidates the putative linear chain of 3 arabinose units and terminal fucose unit linked with (1 → 5) α-glycosidic linkages. This linkage pattern was confirmed by the similar fragmentation pattern noted in the arabinan structure, and terminal fucose was confirmed in correlation with the DP5 fragmentation pattern. The RG-II fraction 2 showed intense peaks around 131.12, 145.19, and 161.05 m/z, corresponding to the ionisation mass pattern of Ara/Xyl, Rha/Fuc, and Gal/Glu, respectively. The overall fragmentation pattern of RG-II fraction 2 was observed to be a complexly branched heteropolymer. The structure of this complex side chain was predicted with the Z ion dominance rule, cross-ring fragmentation peaks, and the probability of having the monosaccharide in correlation with the molar ratio percentage. The molar ratio percentages of the monosaccharide in RG-II fraction 2 give the structural probability of having 4 galactose units, 2 rhamnose units, 2 fucose units, and 1 unit of arabinose, glucose, and xylose in each fraction. When fragmentation peaks have similar ionisation masses of two different monosaccharides, it is assigned to a monosaccharide with a higher molar ratio percentage. The fragmented intensity peak around 217.35 m/z can be ascribed to arabinose/xylose linked with rhamnose/fucose. The first monosaccharide unit is illustrated as arabinose (A_1) from previous reported structural elucidations, and through the fact that arabinose has been reported to have linkages with rhamnose in RG-I and RG-II linear chains (Kaczmarska et al., 2022; Sun et al., 2019; Wu et al., 2018). The second monosaccharide unit was elucidated as rhamnose since the molar percentage ratio of rhamnose is higher than fucose, and it is also evident through the attachments of other monosaccharides as sidechains to rhamnose unit. (Sun et al., 2019) also reported similar sidechain attachments with rhamnose units in their RG sidechains extracted from *Panax ginseng* pectin. Therefore, the fragmentation peak was ascribed to rhamnose (A_2). The first monosaccharide arabinose exhibited the 5th carbon attachment fragmentation pattern, as previously noticed in the RG-I arabinan fraction, evidencing the (5 → 1) α-glycosidic linkage between arabinose and rhamnose. The fragmentation pattern of rhamnose (A_2), three additional possible glycosidic linkages in 2nd (2 → 1), 3rd (3 → 1), and 4th (4 → 1) carbon positions. The fragmentation intensity peak around 379.23 m/z was ascribed to the attachment of galactose with rhamnose. The fragmentation intensity peak around 541.11 m/z was assigned to the attachment of two galactose units. Among these three galactose fragments, two galactoses (X_1) were elucidated as side chains of rhamnose and one galactose (A_3) in linear attachment. This elucidation was predicted in correlation with three possible glycosidic linkages noted in the rhamnose (A_2) unit. Similar side chain arrangements of the rhamnose unit were noted in previous observations of RG fraction made by (Sun et al., 2019). The fragmentation intensity peaks around 687.31 and 849.27 m/z were ascribed to the attachment of terminal fucose (X_2) with galactose side chain and attachment of galactose to rhamnose in a linear pattern, respectively. The fragmentation pattern of fucose-attached galactose showed the possibility of (1 → 4) α-glycosidic linkage. The fragmentation peak around 995.23 was assigned to the attachment of the rhamnose (A_4) unit with galactose (A_3) in a linear pattern. The rhamnose (A_4) also showed three possible glycosidic linkages similar to rhamnose (A_2). The fragmentation peaks around 1157.16 and 1319.41 m/z, representing the side chain attachment pattern of galactose (X_{11}) and glucose (X_{11}) units with possible (1 → 4) β and (1 → 2) α-linkages, respectively. The fragmentation intensity peak around 1451.23 m/z represents the attachment of xylose with either glucose or galactose side chain, with possible (1 → 2) α-linkage. The fragmentation intensity peak, around 1597.18 m/z, can be ascribed to the linear attachment of terminal fucose with the rhamnose unit with possible (1 → 3) β-glycosidic linkage. There are various advantages and limitations to the structural elucidation of polysaccharides done in our study by mass spectrometry analysis. As far as advantages are concerned: 1) the polysaccharide structural elucidation done in this study relied on various factors such as the molar ratio of monosaccharides, previously reported fragmentation patterns of different oligomers and branched polymers, the *Z*-ion dominance rule, and cross-ring cleavage ions. Thus, the probability of having the elucidated structural pattern is high compared to other structural analysis methods, such as NMR; 2) this MS structural analysis method is more suitable and highly reliable for linear polymers even with a high degree of polymerisation and branched polymers with a low degree of polymerisation.

In terms of limitations: 1) to elucidate branched polysaccharides, the monosaccharides with similar mass fragmentation patterns are hard to predict (for example, galactose and glucose), thus the elucidated structure may vary depending on its probability and molar concentration; 2) the linkage assignments for branched polysaccharides through MS cross-ring cleavage ion fragmentation pattern require more study with known structures for facile assignment of bonds.

Fig. 8 illustrates the probable structure of CP in correlation with the observed fragmentation patterns of different RG-I and RG-II side chains.

4. Conclusion

The water and DES-assisted ultrasonication method effectively extracts pectin, extractives and microcellulose (CMC) from citrus wastes (CWs). The glycerol-assisted high-amplitude ultrasonication of CMC was examined as an effective method for the stable production of cellulose nanocrystals. This innovative ultrasonication-based extraction method is anticipated to significantly contribute to the eco-friendly valorisation of CWs within a circular economic framework. Both polar and non-polar extractives of CWs were rich in bioactive compounds and triglycerides of fatty acids, respectively. These bioactive compounds from citrus sources have the potential to serve as antioxidant, antimicrobial, anticancer, and anti-inflammatory agents in various biomedical and food applications. Furthermore, citrus-derived triglycerides can be utilized to produce fatty acids for pharmaceutical ointments, moisturizers, and topical products. The polysaccharides extracted from CWs demonstrated stable physical and chemical properties. The monosaccharide composition analysis and ionisation fragmentation pattern of enzymatically hydrolysed CP fractions elucidated the probable heterosaccharide structures. This detailed structural analysis of complex pectic polysaccharides is expected to advance the state-of-the-art in the structural analysis of branched polysaccharides.

Supplementary data to this article can be found online at https://doi.

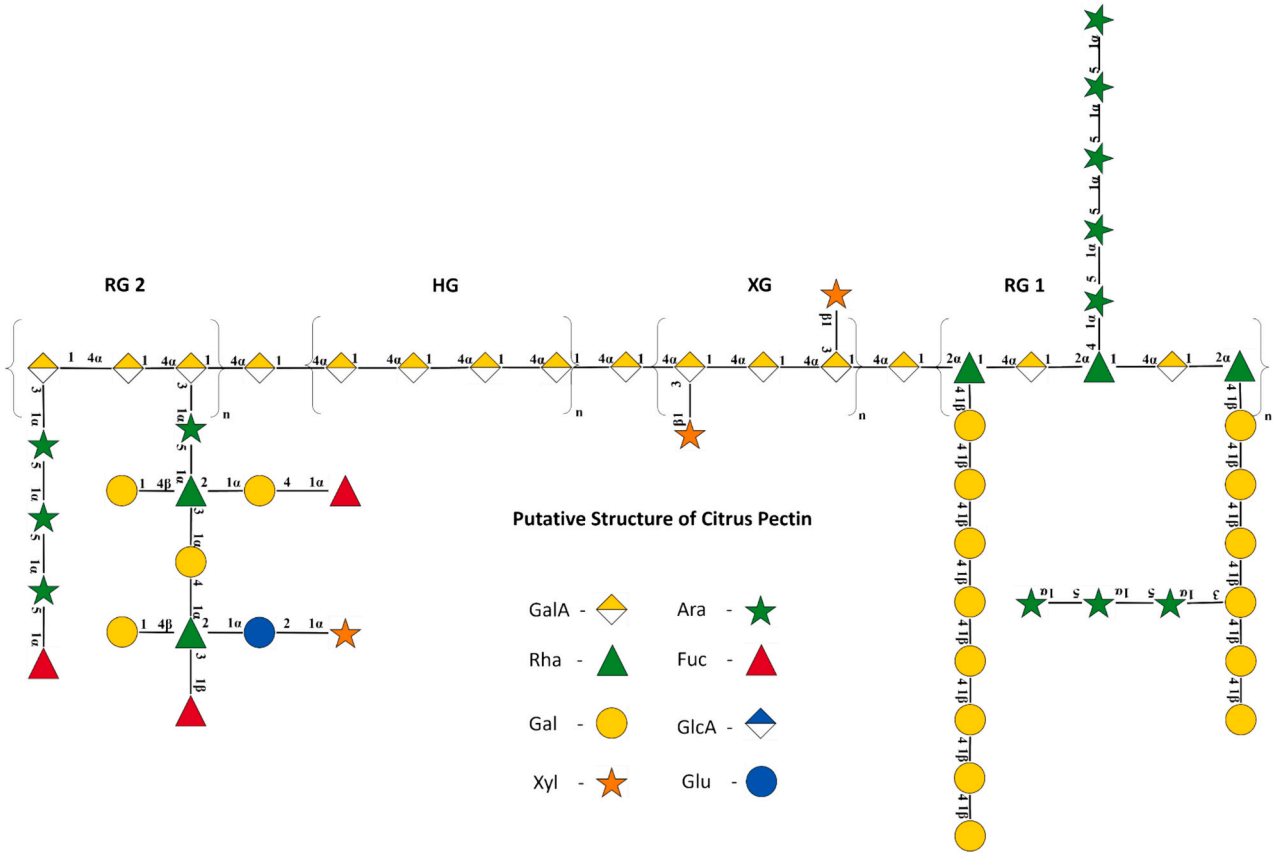

Fig. 8. Putative structure of extracted CP.

org/10.1016/j.carbpol.2024.122539.

CRediT authorship contribution statement

Chandra Mohan Chandrasekar: Writing – original draft, Visualization, Validation, Supervision, Software, Project administration, Methodology, Investigation, Formal analysis, Data curation, Conceptualization. **Daniele Carullo:** Validation. **Francesca Saitta:** Methodology, Formal analysis. **Harini Krishnamachari:** Methodology, Formal analysis. **Tommaso Bellesia:** Formal analysis. **Luca Nespoli:** Formal analysis. **Enrico Caneva:** Formal analysis. **Carlo Baschieri:** Formal analysis. **Marco Signorelli:** Formal analysis. **Alberto Giuseppe Barbiroli:** Formal analysis. **Dimitrios Fessas:** Supervision, Formal analysis. **Stefano Farris:** Writing – review & editing, Supervision, Conceptualization. **Diego Romano:** Writing – review & editing, Validation, Supervision, Resources, Funding acquisition, Conceptualization.

Declaration of competing interest

The authors declare that they have no known competing financial interests or personal relationships that could have appeared to influence the work reported in this paper.

Data availability

Data will be made available on request.

Acknowledgement

The authors acknowledge “ON Foods–Research and innovation network on food and nutrition Sustainability, Safety and Security–Working ON Foods”, PE00000003, Concession Decree No. 1550 of 11 October 2022 adopted by the Italian Ministry of University and Research (National Recovery and Resilience Plan (NRRP), Mission 4 Component 2 Investment 1.3–Call for tender No. 341 of 15 March 2022 of Italian Ministry of University and Research funded by the European Union–Next-GenerationEU). CUP D93C22000890001. The authors also acknowledge the financial support provided by Fondazione Cariplo (Project: CIRCLE, Citrus waste recycling for added value products. 2020–1070), for the implementation of this project.

References

Ai, Y., Yu, Z., Chen, Y., Zhu, X., Ai, Z., Liu, S., & Ni, D. (2016). Rapid determination of the monosaccharide composition and contents in tea polysaccharides from Yingshuang green tea by pre-column derivatization HPLC. *Journal of Chemistry, 2016*. https://doi.org/10.1155/2016/6065813

Al Jitan, S., Scurria, A., Albanese, L., Pagliaro, M., Meneguzzo, F., Zabini, F., Al Sakkaf, R., Yusuf, A., Palmisano, G., & Ciriminna, R. (2022). Micronized cellulose from citrus processing waste using water and electricity only. *International Journal of Biological Macromolecules, 204*, 587–592. https://doi.org/10.1016/j.ijbiomac.2022.02.042

Anari, E. S., Soltanizadeh, N., & Fathi, M. (2024). The potential of DBD plasma pretreatment for the isolation of micro- and nano-cellulose fibers from the walnut shells. *Carbohydrate Polymers, 327*. https://doi.org/10.1016/j.carbpol.2023.121692

Bai, W., Holbery, J., & Li, K. (2009). A technique for production of nanocrystalline cellulose with a narrow size distribution. *Cellulose, 16*(3), 455–465. https://doi.org/10.1007/s10570-009-9277-1

Chandra Mohan, C., Harini, K., Vajiha Aafrin, B., Lalitha Priya, U., Maria Jenita, P., Babuskin, S., … Sukumar, M. (2018). Extraction and characterization of polysaccharides from tamarind seeds, rice mill residue, okra waste and sugarcane bagasse for its bio-thermoplastic properties. *Carbohydrate Polymers, 186*(December 2017), 394–401. https://doi.org/10.1016/j.carbpol.2018.01.057

Chandrasekar, C. M., Nespoli, L., Bellesia, T., Ghaani, M., Farris, S., & Romano, D. (2024). Fabrication of double layer nanoparticle infused starch-based thermoplastic food packaging system for meat preservation. *International Journal of Biological Macromolecules, 254*. https://doi.org/10.1016/j.ijbiomac.2023.127689

Chen, L., Wu, Y., Guo, Y., Yan, X., Liu, W., & Huang, S. (2024). Preparation and characterization of soluble dietary Fiber edible packaging films reinforced by Nanocellulose from navel Orange Peel pomace. *Polymers, 16*(3). https://doi.org/10.3390/polym16030315

Chen, Q., Hu, Z., Yao, F. Y. D., & Liang, H. (2016). Study of two-stage microwave extraction of essential oil and pectin from pomelo peels. *LWT, 66*. https://doi.org/10.1016/j.lwt.2015.11.019

Chen, W., Yu, H., Liu, Y., Hai, Y., Zhang, M., & Chen, P. (2011). Isolation and characterization of cellulose nanofibers from four plant cellulose fibers using a chemical-ultrasonic process. *Cellulose*. https://doi.org/10.1007/s10570-011-9497-z

Cheng, Q., Wang, S., & Rials, T. G. (2009). Poly(vinyl alcohol) nanocomposites reinforced with cellulose fibrils isolated by high intensity ultrasonication. *Composites Part A: Applied Science and Manufacturing.*. https://doi.org/10.1016/j.compositesa.2008.11.009

Chiang, C. F., & Lai, L. S. (2019). Effect of enzyme-assisted extraction on the physicochemical properties of mucilage from the fronds of Asplenium australasicum (J. Sm.) Hook. *International Journal of Biological Macromolecules, 124*, 346–353. https://doi.org/10.1016/j.ijbiomac.2018.11.181

Chu, Y., Sun, Y., Wu, W., & Xiao, H. (2020). Dispersion properties of Nanocellulose: A review. In *, 250. Carbohydrate polymers*. Elsevier Ltd.. https://doi.org/10.1016/j.carbpol.2020.116892

Dogan, M., Aslan, D., & Gurmeric, V. (2018). The rheological behaviors and morphological characteristics of different food hydrocolloids ground to sub-micro particles: In terms of temperature and particle size. *Journal of Food Measurement and Characterization, 12*(2). https://doi.org/10.1007/s11694-017-9691-2

Du, Y., Zhang, S., Sun-Waterhouse, D., Zhou, T., Xu, F., Waterhouse, G. I. N., & Wu, P. (2023). Physicochemical, structural and emulsifying properties of RG-I enriched pectin extracted from unfermented or fermented cherry pomace. *Food Chemistry, 405*. https://doi.org/10.1016/j.foodchem.2022.134985

Du, Y., Zhang, S., Waterhouse, G. I. N., Zhou, T., Xu, F., Wang, R., … Wu, P. (2024). High-intensity pulsed electric field-assisted acidic extraction of pectin from citrus peel: Physicochemical characteristics and emulsifying properties. *Food Hydrocolloids, 146*. https://doi.org/10.1016/j.foodhyd.2023.109291

Einhorn-Stoll, U., Kunzek, H., & Dongowski, G. (2007). Thermal analysis of chemically and mechanically modified pectins. *Food Hydrocolloids, 21*(7). https://doi.org/10.1016/j.foodhyd.2006.08.004

Gong, J., Li, J., Xu, J., Xiang, Z., & Mo, L. (2017). Research on cellulose nanocrystals produced from cellulose sources with various polymorphs. *RSC Advances, 7*, 33486–33493. https://doi.org/10.1039/c7ra06222b

Harini, K., & Chandra Mohan, C. (2020). Isolation and characterization of micro and nanocrystalline cellulose fibers from the walnut shell, corncob and sugarcane bagasse. *International Journal of Biological Macromolecules, 163*, 1375–1383. https://doi.org/10.1016/j.ijbiomac.2020.07.239

Harini, K., Ramya, K., & Sukumar, M. (2018). Extraction of nano cellulose fibers from the banana peel and bract for production of acetyl and lauroyl cellulose. *Carbohydrate Polymers*. https://doi.org/10.1016/j.carbpol.2018.08.081

Humerez-Flores, J. N., Kyomugasho, C., Gutiérrez-Ortiz, A. A., De Bie, M., Panozzo, A., Van Loey, A. M., … Hendrickx, M. E. (2022). Production and molecular characterization of tailored citrus pectin-derived compounds. *Food Chemistry, 367*. https://doi.org/10.1016/j.foodchem.2021.130635

Iranshahi, M., Rezaee, R., Parhiz, H., Roohbakhsh, A., & Soltani, F. (2015). Protective effects of flavonoids against microbes and toxins: The cases of hesperidin and hesperetin. In *, 137. Life sciences* (pp. 125–132). Elsevier Inc.. https://doi.org/10.1016/j.lfs.2015.07.014

Javier-Astete, R., Jimenez-Davalos, J., & Zolla, G. (2021). Determination of hemicellulose, cellulose, holocellulose and lignin content using FTIR in Calycophyllum spruceanum (Benth.) K. Schum. And Guazuma crinita lam. *PLoS ONE, 16*(10 October). doi:https://doi.org/10.1371/journal.pone.0256559.

Juvonen, M., Kotiranta, M., Jokela, J., Tuomainen, P., & Tenkanen, M. (2019). Identification and structural analysis of cereal arabinoxylan-derived oligosaccharides by negative ionization HILIC-MS/MS. *Food Chemistry, 275*, 176–185. https://doi.org/10.1016/j.foodchem.2018.09.074

Kaczmarska, A., Pieczywek, P. M., Cybulska, J., & Zdunek, A. (2022). Structure and functionality of Rhamnogalacturonan I in the cell wall and in solution: A review. In *, 278. Carbohydrate polymers*. Elsevier Ltd.. https://doi.org/10.1016/j.carbpol.2021.118909

Kang, X., Deng, C., Shinde, R., Lin, R., & Murphy, J. D. (2023). Renewable deep eutectic solvents pretreatment improved the efficiency of anaerobic digestion by lignin extraction from willow. *Energy Conversion and Management, 288*. https://doi.org/10.1016/j.enconman.2023.117115

Karimi, K., & Taherzadeh, M. J. (2016). A critical review of analytical methods in pretreatment of lignocelluloses: Composition, imaging, and crystallinity. In *, 200. Bioresource technology* (pp. 1008–1018). Elsevier Ltd.. https://doi.org/10.1016/j.biortech.2015.11.022

Kırcı, D., Demirci, F., & Demirci, B. (2023). Microbial transformation of hesperidin and biological evaluation. *ACS Omega, 8*(45), 42610–42621. https://doi.org/10.1021/acsomega.3c05334

Košťálová, Z., Aguedo, M., & Hromádková, Z. (2016). Microwave-assisted extraction of pectin from unutilized pumpkin biomass. *Chemical Engineering and Processing: Process Intensification, 102*, 9–15. https://doi.org/10.1016/j.cep.2015.12.009

Kouzounis, D., Sun, P., Bakx, E. J., Schols, H. A., & Kabel, M. A. (2022). Strategy to identify reduced arabinoxylo-oligosaccharides by HILIC-MSn. *Carbohydrate Polymers, 289*. https://doi.org/10.1016/j.carbpol.2022.119415

Lemaire, A., Duran Garzon, C., Perrin, A., Habrylo, O., Trezel, P., Bassard, S., … Pelloux, J. (2020). Three novel rhamnogalacturonan I- pectins degrading enzymes from aspergillus aculeatinus: Biochemical characterization and application potential. *Carbohydrate Polymers, 248*. https://doi.org/10.1016/j.carbpol.2020.116752

Lichtenstein, K., & Lavoine, N. (2017). Toward a deeper understanding of the thermal degradation mechanism of nanocellulose. *Polymer Degradation and Stability, 146*. https://doi.org/10.1016/j.polymdegradstab. 2017.09.018

Liew, S. Q., Chin, N. L., Yusof, Y. A., & Sowndhararajan, K. (2016). Comparison of acidic and enzymatic pectin extraction from passion fruit peels and its gel properties. *Journal of Food Process Engineering, 39*(5), 501–511. https://doi.org/10.1111/jfpe.12243

Liew, S. Q., Teoh, W. H., Tan, C. K., Yusoff, R., & Ngoh, G. C. (2018). Subcritical water extraction of low methoxyl pectin from pomelo (Citrus grandis (L.) Osbeck) peels. *International Journal of Biological Macromolecules, 116*, 128–135. https://doi.org/10.1016/j.ijbiomac.2018.05.013

Lin, C. C., Yang, Y. C., Lu, Z. Y., Bagal-Kestwal, D. R., & Lu, T. J. (2022). Profile diversity of galacto-oligosaccharides from disaccharides to hexasaccharides by porous graphitic carbon liquid chromatography-orbitrap tandem mass spectrometry. *Food Chemistry, 390*. https://doi.org/10.1016/j.foodchem.2022.133151

Lin, X., Liu, Y., Wang, R., Dai, J., Wang, L., & Zhang, J. (2024). Extraction of pectins from renewable grapefruit (Citrus paradisi) peels using deep eutectic solvents and analysis of their structural and physicochemical properties. *International Journal of Biological Macromolecules, 254*. https://doi.org/10.1016/j.ijbiomac.2023.127785

Logtenberg, M. J., Donners, K. M. H., Vink, J. C. M., Van Leeuwen, S. S., De Waard, P., De Vos, P., & Schols, H. A. (2020). Touching the high complexity of prebiotic Vivinal Galacto-oligosaccharides using porous graphitic carbon ultra-high-performance liquid chromatography coupled to mass spectrometry. *Journal of Agricultural and Food Chemistry, 68*(29), 7800–7808. https://doi.org/10.1021/acs.jafc.0c02684

Lubinska-Szczygeł, M., Różańska, A., Dymerski, T., Namieśnik, J., Katrich, E., & Gorinstein, S. (2018). A novel analytical approach in the assessment of unprocessed kaffir lime peel and pulp as potential raw materials for cosmetic applications. *Industrial Crops and Products, 120*. https://doi.org/10.1016/j.indcrop.2018.04.036

Mao, Y., Gerrow, A., Ray, E., Perez, N. D., Edler, K., Wolf, B., & Binner, E. (2023). Lignin recovery from cocoa bean shell using microwave-assisted extraction and deep eutectic solvents. *Bioresource Technology, 372*. https://doi.org/10.1016/j.biortech.2023.128680

Mariño, M., Da Silva, L. L., Durán, N., & Tasic, L. (2015). Enhanced materials from nature: Nanocellulose from citrus waste. *Molecules, 20*(4), 5908–5923. https://doi.org/10.3390/molecules20045908

Mariño, M. A., Rezende, C. A., & Tasic, L. (2018). A multistep mild process for preparation of nanocellulose from orange bagasse. *Cellulose, 25*(10), 5739–5750. https://doi.org/10.1007/s10570-018-1977-y

Mathias, D. J., Kumar, S., & Rangarajan, V. (2019). An investigation on citrus peel as the lignocellulosic feedstock for optimal reducing sugar synthesis with an additional scope for the production of hydrolytic enzymes from the aqueous extract waste. *Biocatalysis and Agricultural Biotechnology, 20*. https://doi.org/10.1016/j.bcab.2019.101259

Matsuo, Y., Miura, L. A., Araki, T., & Yoshie-Stark, Y. (2019). Proximate composition and profiles of free amino acids, fatty acids, minerals and aroma compounds in Citrus natsudaidai peel. *Food Chemistry, 279*. https://doi.org/10.1016/j.foodchem.2018.11.146

McDonough, M. A., Kadirvelraj, R., Harris, P., Poulsen, J. C. N., & Larsen, S. (2004). Rhamnogalacturonan lyase reveals a unique three-domain modular structure for polysaccharide lyase family 4. *FEBS Letters, 565*(1–3), 188–194. https://doi.org/10.1016/j.febslet.2004.03.094

Md Salim, R., Asik, J., & Sarjadi, M. S. (2021). Chemical functional groups of extractives, cellulose and lignin extracted from native Leucaena leucocephala bark. *Wood Science and Technology, 55*(2), 295–313. https://doi.org/10.1007/s00226-020-01258-2

Menichini, F., Tundis, R., Bonesi, M., De Cindio, B., Loizzo, M. R., Conforti, F., … Menichini, F. (2011). Chemical composition and bioactivity of Citrus medica L. cv. Diamante essential oil obtained by hydrodistillation, cold-pressing and supercritical carbon dioxide extraction. *Natural Product Research, 25*(8). https://doi.org/10.1080/14786410902900085

Monsoor, M. A., Kalapathy, U., & Proctor, A. (2001). Determination of polygalacturonic acid content in pectin extracts by diffuse reflectance Fourier transform infrared spectroscopy. *Food Chemistry, 74*(2). https://doi.org/10.1016/S0308-8146(01)00100-5

Neckebroeck, B., Verkempinck, S. H. E., Van Audenhove, J., Bernaerts, T., de Wilde d'Estmael, H., Hendrickx, M. E., & Van Loey, A. M. (2021). Structural and emulsion stabilizing properties of pectin rich extracts obtained from different botanical sources. *Food Research International, 141*. https://doi.org/10.1016/j.foodres.2020.110087

Nurdjanah, S., Hook, J., Paton, J., & Paterson, J. (2013). Galacturonic acid content and degree of esterification of pectin from sweet potato starch residue detected using 13 C CP/MAS solid state NMR. In European Journal of Food Research & Review (Vol. 3, Issue 1).

Onkarappa, H. S., Prakash, G. K., Pujar, G. H., Rajith Kumar, C. R., Latha, M. S., & Betageri, V. S. (2020). Hevea brasiliensis mediated synthesis of nanocellulose: Effect of preparation methods on morphology and properties. *International Journal of Biological Macromolecules, 160*. https://doi.org/10.1016/j.ijbiomac.2020.05.188

Panwar, D., Panesar, P. S., & Chopra, H. K. (2023). Ultrasound-assisted extraction of pectin from Citrus limetta peels: Optimization, characterization, and its comparison with commercial pectin. *Food Bioscience, 51*. https://doi.org/10.1016/j.fbio.2022.102231

Panwar, D., Panesar, P. S., & Chopra, H. K. (2024). Green extraction of pectin from Citrus limetta peels using organic acid and its characterization. *Biomass Conversion and Biorefinery, 14*(1), 159–171. https://doi.org/10.1007/s13399-021-02127-z

Pasarin, D., Ghizdareanu, A. I., Teodorescu, F., Rovinaru, C., & Banu, A. (2023). Characterization of pectin oligosaccharides obtained from citrus peel pectin. *Fermentation, 9*(3). https://doi.org/10.3390/fermentation9030312

Patova, O. A., Luanda, A., Paderin, N. M., Popov, S. V., Makangara, J. J., Kuznetsov, S. P., & Kalmykova, E. N. (2021). Xylogalacturonan-enriched pectin from the fruit pulp of

Adansonia digitata: Structural characterization and antidepressant-like effect. *Carbohydrate Polymers, 262*. https://doi.org/10.1016/j.carbpol.2021.117946
Phanthong, P., Ma, Y., Guan, G., & Abudula, A. (2015). Extraction of nanocellulose from raw apple stem. *Journal of the Japan Institute of Energy, 94*(8). https://doi.org/10.3775/jie.94.787
Pitkänen, L., & Sixta, H. (2020). Size-exclusion chromatography of cellulose: Observations on the low-molar-mass fraction. *Cellulose, 27*(16), 9217–9225. https://doi.org/10.1007/s10570-020-03419-9
Prathapan, R., Thapa, R., Garnier, G., & Tabor, R. F. (2016). Modulating the zeta potential of cellulose nanocrystals using salts and surfactants. *Colloids and Surfaces A: Physicochemical and Engineering Aspects, 509*, 11–18. https://doi.org/10.1016/j.colsurfa.2016.08.075
Qi, T., Ren, J., Li, X., An, Q., Zhang, N., Jia, X., Pan, S., Fan, G., Zhang, Z., & Wu, K. (2023). Structural characteristics and gel properties of pectin from citrus physiological premature fruit drop. *Carbohydrate Polymers, 309*. https://doi.org/10.1016/j.carbpol.2023.120682
Rahmani, Z., Khodaiyan, F., Kazemi, M., & Sharifan, A. (2020). Optimization of microwave-assisted extraction and structural characterization of pectin from sweet lemon peel. *International Journal of Biological Macromolecules, 147*, 1107–1115. https://doi.org/10.1016/j.ijbiomac.2019.10.079
Rajulapati, V., Dhillon, A., & Goyal, A. (2021). Enzymatically produced pectic-oligosaccharides from fruit waste of Citrus reticulata (mandarin) peels display cytotoxicity against colon cancer cells. *Bioresource Technology Reports, 15*. https://doi.org/10.1016/j.biteb.2021.100740
Rao, J., Lv, Z., Chen, G., & Peng, F. (2023). Hemicellulose: Structure, chemical modification, and application. *In Progress in Polymer Science, 140*. https://doi.org/10.1016/j.progpolymsci.2023.101675
Rico, X., Gullón, B., & Yáñez, R. (2022). A comparative assessment on the recovery of pectin and phenolic fractions from aqueous and DES extracts obtained from melon peels. *Food and Bioprocess Technology, 15*(6), 1406–1421. https://doi.org/10.1007/s11947-022-02823-2
Rivadeneira, J. P., Wu, T., Ybanez, Q., Dorado, A. A., Migo, V. P., Nayve, F. R. P., & Castillo-Israel, K. A. T. (2020). Microwave-assisted extraction of pectin from "Saba" banana peel waste: Optimization, characterization, and rheology study. *International Journal of Food Science, 2020*. https://doi.org/10.1155/2020/8879425
Rovera, C., Carullo, D., Bellesia, T., Büyüktaş, D., Ghaani, M., Caneva, E., & Farris, S. (2023). Extraction of high-quality grade cellulose and cellulose nanocrystals from different lignocellulosic Agri-food wastes. *Frontiers in Sustainable Food Systems, 6*. https://doi.org/10.3389/fsufs.2022.1087867
Shakhmatov, E. G., Makarova, E. N., & Belyy, V. A. (2019). Structural studies of biologically active pectin-containing polysaccharides of pomegranate Punica granatum. *International Journal of Biological Macromolecules, 122*, 29–36. https://doi.org/10.1016/j.ijbiomac.2018.10.146
Shakhmatov, E. G., Toukach, P. V., & Makarova, E. N. (2020). Structural studies of the pectic polysaccharide from fruits of Punica granatum. *Carbohydrate Polymers, 235*. https://doi.org/10.1016/j.carbpol.2020.115978
Shi, H., Xu, J., Wang, W., Jia, M., Zhou, Y., & Sun, L. (2020a). An efficient protocol for the preparation of linear arabino-oligosaccharides. *Carbohydrate Research, 496*. https://doi.org/10.1016/j.carres.2020.108131
Shi, H., Xu, J., Wang, W., Jia, M., Zhou, Y., & Sun, L. (2020b). An efficient protocol for the preparation of linear arabino-oligosaccharides. *Carbohydrate Research, 496*. https://doi.org/10.1016/j.carres.2020.108131
Siddiqui, A., Chand, K., & Shahi, N. C. (2021). Effect of process parameters on extraction of pectin from sweet lime peels. *Journal of The Institution of Engineers (India): Series A, 102*(2), 469–478. https://doi.org/10.1007/s40030-021-00514-3
Singh, B., Singh, J. P., Kaur, A., & Yadav, M. P. (2021). Insights into the chemical composition and bioactivities of citrus peel essential oils. In *, 143. Food research international*. Elsevier Ltd.. https://doi.org/10.1016/j.foodres.2021.110231
Singhal, S., & Swami Hulle, N. R. (2022). Citrus pectins: Structural properties, extraction methods, modifications and applications in food systems – A review. In Applied Food Research (Vol. 2, Issue 2). Elsevier B.V. doi:https://doi.org/10.1016/j.afres.2022.100215.
Sun, L., Ropartz, D., Cui, L., Shi, H., Ralet, M. C., & Zhou, Y. (2019). Structural characterization of rhamnogalacturonan domains from Panax ginseng C. A. Meyer. *Carbohydrate Polymers, 203*, 119–127. https://doi.org/10.1016/j.carbpol.2018.09.045
TAPPI. (1988). *Acid-insoluble lignin in wood and pulp*. TAPPI Standard T 222 om-88.
Teigiserova, D. A., Tiruta-Barna, L., Ahmadi, A., Hamelin, L., & Thomsen, M. (2021). A step closer to circular bioeconomy for citrus peel waste: A review of yields and technologies for sustainable management of essential oils. In. *Journal of Environmental Management, 280*. https://doi.org/10.1016/j.jenvman.2020.111832
Thomas, P., Duolikun, T., Rumjit, N. P., Moosavi, S., Lai, C. W., Bin Johan, M. R., & Fen, L. B. (2020). Comprehensive review on nanocellulose: Recent developments, challenges and future prospects. In Journal of the Mechanical Behavior of Biomedical Materials (Vol. 110). Elsevier Ltd. doi:https://doi.org/10.1016/j.jmbbm.2020.103884.
Trache, D., Tarchoun, A. F., Derradji, M., Hamidon, T. S., Masruchin, N., Brosse, N., & Hussin, M. H. (2020). Nanocellulose: From fundamentals to advanced applications. In *, 8. Frontiers in chemistry*. Frontiers Media S.A. https://doi.org/10.3389/fchem.2020.00392.
Tsai, S. T., Nguan, H. S., & Ni, C. K. (2021). Identification of anomericity and linkage of arabinose and ribose through collision-induced dissociation. *Journal of Physical Chemistry A, 125*(28), 6109–6121. https://doi.org/10.1021/acs.jpca.1c03854
Updegraff, D. M. (1969). Semimicro determination of cellulose inbiological materials. *Analytical Biochemistry*. https://doi.org/10.1016/S0003-2697(69)80009-6
Varilla-Mazaba, A., Raggazo-Sánchez, J. A., Calderón-Santoyo, M., Gómez-Rodríguez, J., & Aguilar-Uscanga, M. G. (2022). Optimization of lignin extraction by response surface methodology from sugarcane bagasse using deep eutectic solvents (DES). *Industrial Crops and Products, 184*. https://doi.org/10.1016/j.indcrop.2022.115040
Vojvodić Cebin, A., Komes, D., & Ralet, M. C. (2022). Development and validation of HPLC-DAD method with pre-column PMP derivatization for monomeric profile analysis of polysaccharides from agro-industrial wastes. *Polymers, 14*(3). https://doi.org/10.3390/polym14030544
Wang, R., Zhu, X., Qian, W., Hong, Z., Tang, H., Xu, R., & Yu, Y. (2017). Pectin adsorption on amorphous Fe/Al hydroxides and its effect on surface charge properties and Cu(II) adsorption. *Journal of Soils and Sediments, 17*(10). https://doi.org/10.1007/s11368-017-1702-8
Wang, F., Du, C., Chen, J., Shi, L., & Li, H. (2021). A new method for determination of pectin content using spectrophotometry. *Polymers, 13*(17). https://doi.org/10.3390/polym13172847
Wang, J., Liu, Z., Li, X., Liu, G., & Zhao, J. (2023). Elucidating structure of pectin in ramie fiber to customize enzyme cocktail for high-efficiency enzymatic degumming. *Carbohydrate Polymers, 314*. https://doi.org/10.1016/j.carbpol.2023.120954
Wang, W., Ma, X., Jiang, P., Hu, L., Zhi, Z., Chen, J., Ding, T., Ye, X., & Liu, D. (2016). Characterization of pectin from grapefruit peel: A comparison of ultrasound-assisted and conventional heating extractions. *Food Hydrocolloids, 61*. https://doi.org/10.1016/j.foodhyd.2016.06.019
Wani, K. M., & Uppaluri, R. V. S. (2023). Characterization of pectin extracted from pomelo peel using pulsed ultrasound assisted extraction and acidic hot water extraction process. *Applied Food Research, 3*(2). https://doi.org/10.1016/j.afres.2023.100345
Westphal, Y., Kühnel, S., Schols, H. A., Voragen, A. G. J., & Gruppen, H. (2010). LC/CE-MS tools for the analysis of complex arabino-oligosaccharides. *Carbohydrate Research, 345*(15), 2239–2251. https://doi.org/10.1016/j.carres.2010.07.011
Wu, D., Cui, L., Yang, G., Ning, X., Sun, L., & Zhou, Y. (2018). Preparing rhamnogalacturonan II domains from seven plant pectins using Penicillium oxalicum degradation and their structural comparison. *Carbohydrate Polymers, 180*, 209–215. https://doi.org/10.1016/j.carbpol.2017.10.037
Wulandari, W. T., Rochliadi, A., & Arcana, I. M. (2016). Nanocellulose prepared by acid hydrolysis of isolated cellulose from sugarcane bagasse. *IOP Conference Series: Materials Science and Engineering*. https://doi.org/10.1088/1757-899X/107/1/012045
Xia, Y. G., Zhu, R. J., Shen, Y., Liang, J., & Kuang, H. X. (2020). A high methyl ester pectin polysaccharide from the root bark of Aralia elata: Structural identification and biological activity. *International Journal of Biological Macromolecules, 159*, 1206–1217. https://doi.org/10.1016/j.ijbiomac.2020.05.117
Yan, X., Wang, Y., Zhang, Y., Wang, X., Liu, Y., Cui, J., … Cui, L. (2024). Preparation of β-galacto-oligosaccharides using a novel endo-1,4-β-galactanase from Penicillium oxalicum. *International Journal of Biological Macromolecules, 254*. https://doi.org/10.1016/j.ijbiomac.2023.127966
Yapo, B. M., Lerouge, P., Thibault, J. F., & Ralet, M. C. (2007). Pectins from citrus peel cell walls contain homogalacturonans homogenous with respect to molar mass, rhamnogalacturonan I and rhamnogalacturonan II. *Carbohydrate Polymers, 69*(3), 426–435. https://doi.org/10.1016/j.carbpol.2006.12.024
Yi, F., Jin, R., Sun, J., Ma, B., & Bao, X. (2018). Evaluation of mechanical-pressed essential oil from Nanfeng mandarin (Citrus reticulata Blanco cv. Kinokuni) as a food preservative based on antimicrobial and antioxidant activities. *LWT, 95*. https://doi.org/10.1016/j.lwt.2018.05.011
Yu, Y., Wang, Y., Liu, X., Liu, Y., Ji, L., Zhou, Y., & Sun, L. (2021). Comparison of analytical methods for determining methylesterification and acetylation of pectin. *Applied Sciences (Switzerland), 11*(10). https://doi.org/10.3390/app11104461
Zhu, X., Liu, B., Zheng, S., & Gao, Y. (2014). Quantitative and structure analysis of pectin in tobacco by 13C CP/MAS NMR spectroscopy. *Analytical Methods, 6*(16), 6407–6413. https://doi.org/10.1039/c4ay01156b
Zhuang, H., Chu, S., Wang, P., Zhou, B., Han, L., Yu, X., Fu, Q., & Li, S. (2019). Study on the emulsifying properties of pomegranate peel pectin from different cultivation areas. *Molecules, 24*(9). https://doi.org/10.3390/molecules24091819